On the Impact of Warden Collusion on Covert Communication in Wireless Networks

Shuangrui Zhao, *Member, IEEE,* Jia Liu, *Senior Member, IEEE,* Yulong Shen, *Member, IEEE,* Xiaohong Jiang, *Senior Member, IEEE,* Tarik Taleb, *Senior Member, IEEE,* and Norio Shiratori, *Life Fellow, IEEE*

***Abstract*—Warden collusion represents a hazardous threat to wireless covert communication, where wardens can combine their observations to perform a more aggressive detection attack. This paper investigates the impact of warden collusion on covert communication in a multi-antenna wireless network consisting of one source, one destination, multiple wardens and interferers. By employing the techniques of Laplace Transform and Cauchy Integral Theorem, we first establish a framework to model the aggregate interference distribution (AID) for covert communication in the network under the typical additive white Gaussian noise (AWGN) and Rayleigh fading channels. Based on the AID results, we then develop theoretical models to reveal the inherent relationship between the collusion intensity and fundamental communication metrics in terms of the covert outage probability, connection outage probability and covert throughput. With the help of these models, we further explore the covert throughput optimization problems and present extensive numerical results to illustrate the impact of warden collusion on the covert throughput under both channel models.**

***Index Terms*—Warden collusion, covert communication, collusion intensity, outage probability, covert throughput.**

I. Introduction

Security and privacy of wireless communications have always been critical considerations for network operators due to the broadcast nature of the wireless medium. Although available methods based on cryptography or physical layer security have been successful in preventing the wireless information from being intercepted by illegitimate receivers, malicious wardens can still detect the existence of communications so as to launch attacks to legitimate users [1], [2]. Actually, in many real-life instances like unmanned aerial vehicle (UAV) networks and submarine communications, protecting only the confidentiality of communication contents is insufficient and users there may desire to transfer information covertly. This motivates the studies of covert communication, which aims to hide the very existence of wireless transmission itself from potential wardens [3].

A. Literature Review

While covert communication was traditionally implemented by exploiting the spread spectrum techniques [4], recent studies indicated that physical layer security (PLS) serves as an attractive approach to ensure covert communication [5]. In particular, lots of works have been devoted to the study of PLS-based covert communications in a single warden system with a transmitter Alice, a receiver Bob and a warden Willie. Bash *et al.* [6] first revealed a square root law for the additive white Gaussian noise (AWGN) channels, which indicates that for n channel uses at most $O(\sqrt{n})$ information bits can be reliably and covertly transmitted to a target receiver against a warden. Later, the covert communication in single warden systems was examined under various PLS techniques, like the background noise [7]–[11], artificial noise [12]–[15] and beamforming [16]–[19].

To explore the benefits of relaying in covert communications, the single warden model with cooperative relay has also been widely adopted. In [20], the authors considered a relay system under AWGN channels where a cooperative relay seeks to covertly send its message to the destination using the communications resources allocated by the source, and then explored the impact of the relay on the covert rate in the system. Wang *et al.* [21] exploited the application of beamforming on the covert communication in a decode-and-forward relay system, while Deng *et al.* [22] applied the artificial noise technique to design a covert communication scheme for an intelligent reflecting surface assisted relay system under Rayleigh fading channels. Later, Gao *et al.* [23] examined a more general multi-relay system under Rayleigh fading channels and conducted a related theoretical analysis on the covert communication performance of the system in terms of detection probability and covert capacity. Under Rayleigh fading channels, Lin *et al.* [24] investigated covert communication in a finite block-length system with one multi-antenna relay, while Wang *et al.* [25] developed a framework to analyze covert performance under decode-and-forward protocols and the optimal setting of warden's detection threshold.

This work was supported in part by the National Key R&D Program of China under Grant 2023YFB3107500, in part by the Major Research plan of the National Natural Science Foundation of China under Grant 92267204, in part by the National Natural Science Foundation of China under Grant 62202355, 62220106004, in part by the Key Research and Development Program of Shaanxi (Program No. 2024GX-YBXM-028), in part by the Technology Innovation Leading Program of Shaanxi (No. 2022KXJ-093, 2023KXJ-033), in part by the Innovation Capability Support Program of Shaanxi (No. 2023-CX-TD-02), in part by the Fundamental Research Funds for the Central Universities (No. ZDRC2202), in part by the European Union's HE Research and Innovation Program HORIZON-JUSNS-2023 through the 6G-Path Project under Grant 101139172, and in part by the Cooperative Research Project Program of the Research Institute of Electrical Communication, Tohoku University. *(Corresponding authors: Jia Liu; Yulong Shen.)*

S. Zhao, J. Liu and Y. Shen are with the School of Computer Science and Technology, Xidian University, Xi'an, 710071 China (e-mail: zhaoshuangrui@xidian.edu.cn, liujia@xidian.edu.cn, ylshen@mail.xidian.edu.cn).

X. Jiang is with the School of Systems Information Science, Future University Hakodate, Hakodate, 041-8655 Japan (e-mail: jiang@fun.ac.jp).

T. Taleb is with Ruhr University Bochum, Bochum, 44801 Germany (e-mail: tarik.taleb@rub.de).

N. Shiratori is with the Research and Development Initiative, Chuo University, Tokyo, 112-8551 Japan (email: norio@riec.tohoku.ac.jp).

Recently, some initial studies have been conducted to further investigate the covert communication in multiple warden systems [26]–[28]. Ma *et al.* [26] investigated the joint designs of transmit power and block-length for covert communication in a multi-antenna system with multiple randomly located wardens. Jiang *et al.* [27] considered the covert throughput maximization for covert communication in a wireless energy harvesting-enabled cellular network with multiple wardens, where the power beacons serve as friendly jammers to send jamming signals to confuse the wardens. For covert communication in a large-scale device-to-device communication system with multiple wardens, Feng *et al.* [28] proposed a Stackelberg game approach to analyze the tradeoff between the wardens' detection error probability and transmitters' secrecy outage probability under Rayleigh fading channels.

The aforementioned works help us to gain the basic understandings of covert communication in various communication scenarios. Note that to simplify the analysis, these works consider either the scenarios of a single warden or multiple but non-colluding wardens, where each warden works independently to detect the existence of communication using only his own observation. In practice, however, warden collusion represents a hazardous threat to covert communication, where multiple wardens can combine their observations to perform a more aggressive detection attack. Some initial works on the covert communications under warden collusion can be found in [29]–[32]. Specifically, Zhao *et al.* [29] studied the efficient approximation of covert outage performance in a circular random network with AWGN channels and multiple fully colluding wardens. In [30], Ma *et al.* analyzed the average covert throughput performance in a multiple warden system with fully colluding detection and Rayleigh fading channels, and demonstrated that the covert performance in the system can be improved by enlarging the blocklength only when the density of the wardens is small. In [31], Arghavani *et al.* focused on the covert communication in a Rayleigh fading system with a source, a destination, a jammer and multiple fully colluding wardens, and proposed a zero-sum game to study the tradeoff between the detection error probability at the wardens and the covert outage probability at the destination. Jia *et al.* [32] considered the covert transmission in an integrated sensing and communication system with multiple wardens and Rician channels, and designed the robust beamforming schemes for covert transmissions under both non-colluding and fully colluding warden scenarios.

B. Novelty and Contributions

As a step further towards the study of covert communication under general warden collusion scenarios, this paper focuses on a multi-antenna network consisting of one source, one destination, multiple randomly distributed wardens and interferers, and applies a general warden collusion model to investigate the impact of warden collusion on achievable covert communication performance in the network. Note that the AWGN and Rayleigh fading channels can effectively capture the impact of noise and multipath fading in different communication environments, so they serve as the representative models in available works on covert communications across different scenarios [28]–[31]. Therefore, we also adopt these two channel models in our analysis to ensure the relevance and generalizability of our results.

The contributions of this paper are summarized as follows.

- We consider a general $(m, M)-$colluding model for covert communication, where any m of all M wardens can combine their observations to perform transmission detection. The model is general in the sense it covers the scenarios of a single warden $(m = M = 1)$, non-colluding wardens $(m = 1, M > 1)$ and full-colluding wardens $(m = M > 1)$ as special cases.
- We establish a framework to model the aggregate interference for covert communication in the wireless network under the typical AWGN and Rayleigh fading channel models. By adopting the techniques of Laplace transform and Cauchy Integral Theorem, we derive the probability density function (PDF) and cumulative distribution function (CDF) of the aggregate interference at both non-colluding and colluding wardens.
- Based on the aggregate interference distribution (AID) results, we analyze the average detection probabilities of the non-colluding and colluding wardens. The expressions for the covert outage probability, connection outage probability, and covert throughput are then derived to reveal the inherent relationship between the collusion intensity m and these fundamental metrics.
- To understand the impact of warden collusion on the maximal covert throughput, we further explore the joint optimal design of transmit power and transmission rate for the covert throughput maximization subject to given requirements on the covert outage.
- Extensive simulation and numerical results are provided to illustrate our theoretical findings and demonstrate that warden collusion may significantly deteriorate the performance of covert communication.

The rest of this paper is organized as follows. Section II introduces the system model. The impact of the warden collusion under AWGN and Rayleigh fading channels are presented in Section III and Section IV, respectively. Numerical results are provided in Section V, followed by the conclusion in Section VI.

Notations: Column vectors are denoted by lower-case boldface. The absolute value, Euclidean norm, conjugate, transpose, Hermitian transpose, natural logarithm, probability, and the expectation are denoted, respectively, by $|\cdot|$, $||\cdot||$, $(\cdot)^{\dagger}$, $(\cdot)^{'}$, $(\cdot)^{H}$, $\ln(\cdot)$, $\mathbb{P}\{\cdot\}$ and $\mathbb{E}[\cdot]$. The PDF and CDF of a are denoted by $f_a(\cdot)$ and $\mathcal{F}_a(\cdot)$, respectively.

II. System Model

A. $(m, M)-$Colluding Model

We consider a multi-antenna covert communication system consisting of a source Alice, a destination Bob, M wardens $W_1, W_2, \ldots, W_M$, and numerous independent interferers, as depicted in Fig. 1. Alice is equipped with N_A antennas while all the other nodes including Bob, the wardens, and interferers are equipped with a single antenna. Alice intends to transmit

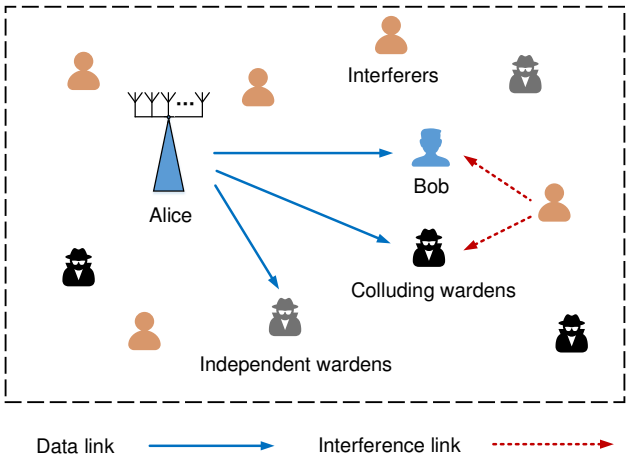

Fig. 1. Illustration of a multi-antenna covert communication system under warden collusion. Alice intends to communicate with Bob while guaranteeing a low probability of being detected by M wardens ($M = 5$ in the figure). The wardens work in a colluding manner such that any m wardens can combine their available observations to conduct more powerful detection ($m = 3$ in the figure). The numerous interferers are randomly located in the network (five interferers in the figure).

messages to Bob covertly, while wardens aim to detect whether Alice has transmitted information signals or not.

Based on the wardens' behavior, we focus on a $(m, M)-$colluding warden scenario in which any m wardens (i.e., W_1, W_2, ..., W_m, $1 \leq m \leq M$) can combine their available observations to detect the transmission. The notation m is referred to as the collusion intensity to quantify the degree of warden collusion. For a group of m colluding wardens, one of them will serve as the super warden W_Z, which has the information of individually received signal energy of each of these m wardens. Notice that in this paper, we assume that each warden has only the statistical channel state information (CSI) rather than the instantaneous CSI for the channel from Alice to itself, so we employ the equal gain combining (EGC) technique in W_Z to achieve colluding detection [33], where W_Z combines the received signal energy of these m wardens by summing them to determine whether Alice is transmitting. The EGC owns the advantages of lower computational complexity and no requirement for instantaneous CSI for Alice-warden links, making it suitable for scenarios where only statistical CSI is available. By now, the EGC technique has been widely applied to covert communication and signal detection systems (see, for example, [33]–[35]). Note that the $(m, M)-$colluding model is relevant in practical applications, as it flexibly simulates different levels of collusion among wardens in various scenarios. For example, in mobile networks, multiple base stations deployed across regions detect unauthorized signals. When an illegal base station is suspected in a specific area, a subset of base stations (e.g., m out of M) may be activated to perform colluding detection, while the rest operate independently to maintain regular communication services for legitimate users [36].

We consider a two-dimensional network where the locations of Alice and Bob are fixed, and the locations of the wardens follow a static uniform distribution. In particular, we randomly place the independent interferers at the network such that the distribution of their locations follows a homogeneous Poisson point process Φ with density λ. We denote the locations of Alice, Bob, the warden W_x, and the interferer $I_{\rm y}$ as $\mathbb{L}_A$, $\mathbb{L}_B$, $\mathbb{L}_{W_x}$, and $\mathbb{L}_{I_{\rm y}}$, respectively. We assume that Alice (resp. Bob) knows the location of Bob (resp. Alice) but not the locations of the wardens and independent interferers, and the wardens know the locations of Alice and Bob but not the locations of the interferers. Regarding the CSI assumptions relevant to this study, Alice and Bob have access to the instantaneous CSI of the main channel from Alice to Bob, which can be obtained through pilot-based channel estimation between them [37]. However, due to the lack of cooperative communication between Alice/Bob and the wardens/interferers, Alice does not have the CSI for her channels to the wardens and Bob does not have the CSI for the channels from the interferers to himself. Also, each warden does not have the CSI for the channels from the interferers to itself, but has only the statistical CSI for the channel from Alice to itself, which can be derived from the long-term observations of environmental fading [38].

All wireless links are modeled as quasi-static and statistical independent channels with distance-based path loss exponent α, that is, the channel fading coefficient of each link remains constant during one time slot. The channel coefficients from the source Alice and the interferer $I_{\rm y}$ to the destination Bob are denote as $\mathbf{h}_{A,B} \in \mathbb{C}^{N_A \times 1}$ and $h_{I_{\rm y},B}$, respectively. The channel coefficients from Alice and the interferer $I_{\rm y}$ to the warden W_x are denote as $\mathbf{h}_{A,W_x} \in \mathbb{C}^{N_A \times 1}$ and $h_{I_{\rm y},W_x}$, respectively. The distance from Alice and the interferer $I_{\rm y}$ to Bob are denote as $d_{A,B}$ and $d_{I_{\rm y},B}$, respectively. The distance from Alice and the interferer $I_{\rm y}$ to W_x are denote as d_{A,W_x} and $d_{I_{\rm y},W_x}$, respectively. We consider the interference-limited network scenario widely adopted in literature [39]–[41], where the signals from multiple interferers accumulate incoherently at a receiver (e.g., Bob, warden), leading to a total interference power much greater than the thermal noise power at the receiver. Therefore, we ignore the thermal noise at both Bob and wardens in our analysis.

Since Alice knows neither the locations of the wardens nor the CSI for her channels to the wardens, Alice is not able to design optimal beamforming to transmit in the null space of the channels from Alice to all wardens to ensure perfect covertness. However, with the information of the location of Bob and the instantaneous CSI of the main channel from Alice to Bob, Alice can leverage the maximum ratio transmission (MRT) to ensure a signal strength advantage toward Bob while significantly degrading the signal at the wardens. Notice also that each warden has only the statistical CSI for the channel from Alice to itself and does not have the CSI for the channels from interferers to itself, so the covertness constraint can be jointly ensured by the degraded signals from Alice to the wardens as well as the uncertainties of the Alice-warden channels and interference signals from the interferers.

When Alice transmits a normalized signal $s[k] \sim \mathcal{CN}(0, 1)$ with MRT beamforming, the received signal $y_B[k]$ at Bob is

given by

$$y_B[k] = \sqrt{P_A}\mathbf{g}_A\mathbf{h}_{A,B}d_{A,B}^{-\alpha/2}s[k] + \sum_{\mathbb{L}_{I_\mathrm{y}}\in\Phi}\sqrt{P_I}h_{I_\mathrm{y},B}d_{I_\mathrm{y},B}^{-\alpha/2}n_{I_\mathrm{y}}[k], \quad (1)$$

where P_A denotes the transmit power of Alice, P_I denotes the common transmit power of each interferer, $n_{I_\mathrm{y}}[k]$ denotes the interference signal from the interferer I_y, and $\mathbf{g}_A = \frac{\mathbf{h}_{A,B}^H}{||\mathbf{h}_{A,B}||}$ is the weight vector. Similarly, the received signal $y_{W_j}[k]$ at the warden W_j ($j \in \{m+1, m+2, \ldots, M\}$) is given by

$$y_{W_j}[k] = \sqrt{P_A}\mathbf{g}_A\mathbf{h}_{A,W_j}d_{A,W_j}^{-\alpha/2}s[k] + \sum_{\mathbb{L}_{I_\mathrm{y}}\in\Phi}\sqrt{P_I}h_{I_\mathrm{y},W_j}d_{I_\mathrm{y},W_j}^{-\alpha/2}n_{I_\mathrm{y}}[k]. \quad (2)$$

In the $(m, M)-$colluding scenario with m colluding wardens ($W_1, \ldots, W_v, \ldots, W_m, v \in \{1, 2, \ldots, m\}$) and the EGC technique, the received signal $y_Z[k]$ at super warden W_Z is given by

$$y_Z[k] = \sum_{v=1}^{m}(\sqrt{P_A}\mathbf{g}_A\mathbf{h}_{A,W_v}d_{A,W_v}^{-\alpha/2}s[k] + \sum_{\mathbb{L}_{I_\mathrm{y}}\in\Phi}\sqrt{P_I}h_{I_\mathrm{y},W_v}d_{I_\mathrm{y},W_v}^{-\alpha/2}n_{I_\mathrm{y}}[k]). \quad (3)$$

B. Detection Model

In order to detect the presence of the covert communication, wardens have to distinguish between the following two hypotheses:

$$\mathcal{H}_0 : \begin{cases} y_{W_j}[k] = \sum_{\mathbb{L}_{I_\mathrm{y}}\in\Phi}\sqrt{P_I}h_{I_\mathrm{y},W_j}d_{I_\mathrm{y},W_j}^{-\alpha/2}n_{I_\mathrm{y}}[k], \\ y_Z[k] = \sum_{v=1}^{m}\sum_{\mathbb{L}_{I_\mathrm{y}}\in\Phi}\sqrt{P_I}h_{I_\mathrm{y},W_v}d_{I_\mathrm{y},W_v}^{-\alpha/2}n_{I_\mathrm{y}}[k], \end{cases} \quad (4)$$

$$\mathcal{H}_1 : \begin{cases} y_{W_j}[k] = \sqrt{P_A}\mathbf{g}_A\mathbf{h}_{A,W_j}d_{A,W_j}^{-\alpha/2}s[k] \\ \qquad + \sum_{\mathbb{L}_{I_\mathrm{y}}\in\Phi}\sqrt{P_I}h_{I_\mathrm{y},W_j}d_{I_\mathrm{y},W_j}^{-\alpha/2}n_{I_\mathrm{y}}[k], \\ y_Z[k] = \sum_{v=1}^{m}(\sqrt{P_A}\mathbf{g}_A\mathbf{h}_{A,W_v}d_{A,W_v}^{-\alpha/2}s[k] \\ \qquad + \sum_{\mathbb{L}_{I_\mathrm{y}}\in\Phi}\sqrt{P_I}h_{I_\mathrm{y},W_v}d_{I_\mathrm{y},W_v}^{-\alpha/2}n_{I_\mathrm{y}}[k]), \end{cases} \quad (5)$$

where the null hypothesis $\mathcal{H}_0$ indicates that Alice has not transmitted signals, while the alternate hypothesis $\mathcal{H}_1$ means that Alice has transmitted.

A correct detection for the wardens is to accept $\mathcal{H}_0$ when it is true and reject $\mathcal{H}_0$ when it is false. The decision rule for the wardens W_j and W_Z can be respectively expressed as [42]

$$\begin{cases} \overline{P}_{W_j} = \frac{1}{K}\sum_{k=1}^{K}|y_{W_j}[k]|^2 \le \xi_1, & \mathcal{D}_0 \\ \overline{P}_{W_j} = \frac{1}{K}\sum_{k=1}^{K}|y_{W_j}[k]|^2 > \xi_1, & \mathcal{D}_1 \end{cases} \quad (6)$$

and

$$\begin{cases} \overline{P}_Z = \frac{1}{K}\sum_{k=1}^{K}|y_Z[k]|^2 \le \xi_2, & \mathcal{D}_0 \\ \overline{P}_Z = \frac{1}{K}\sum_{k=1}^{K}|y_Z[k]|^2 > \xi_2, & \mathcal{D}_1 \end{cases} \quad (7)$$

where $\overline{P}_{W_j}$ and $\overline{P}_Z$ are the average power of the received signals at W_j and W_Z, respectively, K is the number of channel uses in each time slot, ξ_1 and ξ_2 are the predefined detection thresholds for the detectors of W_j and W_Z, respectively, $\mathcal{D}_0$ and $\mathcal{D}_1$ are the binary decisions corresponding to $\mathcal{H}_0$ and $\mathcal{H}_1$, respectively. The decision $\mathcal{D}_0$ or $\mathcal{D}_1$ for W_j is made based on whether $\overline{P}_{W_j} \le \xi_1$ or $\overline{P}_{W_j} > \xi_1$. Similarly, the decision $\mathcal{D}_0$ or $\mathcal{D}_1$ for W_Z is made based on whether $\overline{P}_Z \le \xi_2$ or $\overline{P}_Z > \xi_2$.

Following the widely-adopted assumption in the previous studies on covert communication, we assume that all wardens can receive an infinite number of samples, i.e., $K \to \infty$. Thus, the average power of the received signals at W_j and W_Z are reformulated as

$$\mathcal{H}_0 : \begin{cases} \overline{P}_{W_j} = V_{W_j}, \\ \overline{P}_Z = \sum_{v=1}^{m} V_{W_v}, \end{cases} \quad (8)$$

$$\mathcal{H}_1 : \begin{cases} \overline{P}_{W_j} = U_{W_j} + V_{W_j}, \\ \overline{P}_Z = \sum_{v=1}^{m}(U_{W_v} + V_{W_v}), \end{cases} \quad (9)$$

where $U_{W_x} = P_A\mathbf{g}_A\mathbf{h}_{A,W_x}\mathbf{h}_{A,W_x}^H\mathbf{g}_A^H d_{A,W_x}^{-\alpha}$ and $V_{W_x} = \sum_{\mathbb{L}_{I_\mathrm{y}}\in\Phi}|\sqrt{P_I}h_{I_\mathrm{y},W_x}d_{I_\mathrm{y},W_x}^{-\alpha/2}|^2$ for $x \in \{j, v\}$ are the power of the received signals from Alice and the interferers, respectively.

For simplicity, we set the prior probabilities of hypotheses $\mathcal{H}_0$ and $\mathcal{H}_1$ as $\mathbb{P}\{\mathcal{H}_0\} = \mathbb{P}\{\mathcal{H}_1\} = \frac{1}{2}$. Then, the correct detection probabilities p_{W_j} and p_Z at W_j and W_Z can be respectively calculated as

$$p_{W_j} = \mathbb{P}\{\mathcal{H}_0\}\mathbb{P}\{\overline{P}_{W_j} \le \xi_1|\mathcal{H}_0\} + \mathbb{P}\{\mathcal{H}_1\}\mathbb{P}\{\overline{P}_{W_j} > \xi_1|\mathcal{H}_1\} = \begin{cases} 1, & V_{W_j} \le \xi_1 < U_{W_j} + V_{W_j}, \\ \frac{1}{2}, & \text{otherwise}, \end{cases} \quad (10)$$

and

$$p_Z = \mathbb{P}\{\mathcal{H}_0\}\mathbb{P}\{\overline{P}_Z \le \xi_1|\mathcal{H}_0\} + \mathbb{P}\{\mathcal{H}_1\}\mathbb{P}\{\overline{P}_Z > \xi_1|\mathcal{H}_1\} = \begin{cases} 1, & \sum_{v=1}^{m} V_{W_v} \le \xi_2 < \sum_{v=1}^{m}(U_{W_v} + V_{W_v}), \\ \frac{1}{2}, & \text{otherwise}. \end{cases} \quad (11)$$

where $p_{W_j} = p_Z = 1$ indicates that the detection of the wardens is successful, while $p_{W_j} = p_Z = \frac{1}{2}$ indicates that the detection is failed [41].

We can see from (10) and (11) that the parameters involved in these equations are the channel CSI $\mathbf{h}_{A,W_x}$ and distance d_{A,W_x} from Alice to warden W_x ($x \in \{j, v\}$), the MRT weight vector $\mathbf{g}_A$ and transmission power P_A of Alice, transmission power P_I of interferers, as well as the channel CSI h_{I_y,W_x} and distance d_{I_y,W_x} from interferer I_y to warden W_x. From our assumptions on CSI and location availability, we can see that warden W_x has the knowledge of d_{A,W_x} and the statistical distribution for $\mathbf{h}_{A,W_x}$, but has no knowledge about $\mathbf{g}_A$, P_A, P_I, h_{I_y,W_x}, and d_{I_y,W_x}. It is notable that for the warden W_x, its uncertainties on $\mathbf{h}_{A,W_x}$, $\mathbf{g}_A$ and P_A cause its uncertainty on signal from Alice while its uncertainties on P_I, h_{I_y,W_x} and d_{I_y,W_x} cause its uncertainty on signal from I_y, and such signal uncertainties will finally lead to the randomness in its detection.

Remark 1: For the scenario where the instantaneous CSI for the channel from Alice to each colluding warden is available at W_Z, the maximum ratio combining (MRC) can be another

important technique for multi-warden colluding detection, in which the super warden W_Z can maximize the overall signal-to-noise ratio (SNR) by optimally weighting the received signal at each colluding warden based on the instantaneous CSI from Alice to the warden, thereby enhancing the detection capability of W_Z [32]. In the context when each warden knows the instantaneous CSI from Alice to itself, with the MRC the final signal $y_Z[k]$ at W_Z can be represented as

$$y_Z[k] = \sum_{v=1}^{m} \iota_v (\sqrt{P_A}\mathbf{g}_A \mathbf{h}_{A,W_v} d_{A,W_v}^{-\alpha/2} s[k] + \sum_{\mathbb{L}_{I_y} \in \Phi} \sqrt{P_I} h_{I_y,W_v} d_{I_y,W_v}^{-\alpha/2} n_{I_y}[k]), \quad (12)$$

where $\iota_v = \frac{\mathbf{h}_{A,W_v}^H}{\|\mathbf{h}_{A,W_v}^H\|^2}$ is the weighting factor for each channel. Thus, the correct detection probability p_Z at W_Z in (11) can be rewritten as

$$p_Z = \begin{cases} 1, \ \sum_{v=1}^{m} \iota_v^2 V_{W_v} \leq \xi_2 < \sum_{v=1}^{m} \iota_v^2 (U_{W_v} + V_{W_v}), \\ \frac{1}{2}, \ \text{otherwise.} \end{cases} \quad (13)$$

Let $\vartheta = \iota_v^2 V_{W_v}$ denote the aggregate interference. Then, the PDF of ϑ, denoted by $f_\vartheta(\vartheta)$, can be expressed as

$$f_\vartheta(\vartheta) = \int_{-\infty}^{\infty} f_{\iota_v^2}(x) \cdot f_{V_{W_v}}\left(\frac{\vartheta}{x}\right) \frac{1}{|x|}\, dx. \quad (14)$$

Since the locations of the interferers are modeled by a homogeneous poisson point process, the interference V_{W_v} is represented as shot noise, whose distribution function can only be expressed as an infinite series [43]. We observe that when each element of $\mathbf{h}_{A,W_v}$ follows a Rayleigh distribution, it is extremely difficult to derive closed-form solutions for the PDF and CDF of the aggregate interference ϑ. As a result, obtaining closed-form expressions for the covert outage probability proves to be highly difficult. However, we can still apply Monte-Carlo simulation in Section V to illustrate the detection performance under the MRC technique.

C. Performance Metrics

In order to study the impact of the warden collusion on the covert communication, we introduce the following fundamental covert communication metrics.

1) Covert Outage Probability: We invoke the concept of the covert outage event to characterize the covert performance of the system. The covert outage event occurs when the covert communication from Alice to Bob is detected by the wardens W_j or W_Z. The probability of this event happening is referred to as the covert outage probability, denoted as $\mathcal{P}_{cov}$. According to (10) and (11), the covert outage probability $\mathcal{P}_{cov}$ is given by

$$\mathcal{P}_{cov} = \mathbb{P}\left\{ \bigcup_{j=m+1}^{M} p_{W_j} = 1 \quad \text{or} \quad p_Z = 1 \right\}. \quad (15)$$

2) Connection Outage Probability: A signal received at Bob can not be successfully decoded if the channel capacity from Alice to Bob is less than the predefined transmission rate R, and we say that the connection outage event happens. The probability that this event happens is referred to as the connection outage probability. Based on the expression (1), the SNR of the channel from Alice to Bob is expressed as

$$SNR_{A,B} = \frac{U_B}{V_B}, \quad (16)$$

where $U_B = P_A d_{A,B}^{-\alpha} ||\mathbf{h}_{A,B}||^2$ is the power of the desired signal from Alice and $V_B = \sum_{\mathbb{L}_{I_y} \in \Phi} P_I d_{I_y,B}^{-\alpha} |h_{I_y,B}|^2$ is the aggregate interference power from interferers. Let C_B denote the channel capacity. From (16), we have $C_B = \log_2(1 + SNR_{A,B})$ bps/Hz. Therefore, the connection outage probability $\mathcal{P}_{con}$ can be calculated as

$$\mathcal{P}_{con} = \mathbb{P}\{C_B < R\} = \mathbb{P}\{SNR_{A,B} < \beta\}, \quad (17)$$

where $\beta = 2^R - 1$ is the SNR threshold.

3) Covert Throughput: In this paper, we adopt the covert throughput to evaluate the rate efficiency of the covert communication. Covert throughput refers to the rate of successfully transmitted information per second per Hertz, while satisfying a given constraint on covert outage probability. This metric represents the maximum data rate that the transmitter can achieve in covert communication. Mathematically, the covert throughput η can be expressed as

$$\eta = (1 - \mathcal{P}_{con})R, \quad \mathcal{P}_{cov} \leq \epsilon, \quad (18)$$

where ϵ is the maximal acceptable threshold of covert outage probability.

III. Warden Collusion Under AWGN Channel

In this section, we study the impact of warden collusion on the covert communication under AWGN channels. In particular, we first model the aggregate interference distribution, and then derive the covert outage probability and connection outage probability. The covert throughput is further maximized by jointly designing Alice's transmit power and transmission rate.

A. Aggregate Interference Distribution

Revisiting the detection strategy at W_j and W_Z described in Section II, we note that the major obstacle of calculating $\mathcal{P}_{cov}$ lies in the aggregate interference power V_{W_j} and $\sum_{v=1}^{m} V_{W_v}$. According to the results in [44], the Laplace transform of V_{W_j} evaluated at s can be expressed as

$$\mathcal{L}_{V_{W_j}}(s) = \mathbb{E}_{V_{W_j}}[e^{-sV_{W_j}}] = e^{-\rho s^{\frac{2}{\alpha}}}, \quad (19)$$

where $\rho = \pi\lambda\Gamma(1 - \frac{2}{\alpha})P_I^{\frac{2}{\alpha}}$. Next, we provide the PDF of V_{W_j} in the following lemma.

Lemma 1: The PDF $f_{V_{W_j}}(x)$ of the total aggregate interference V_{W_j} at W_j is given by

$$f_{V_{W_j}}(x) = \frac{1}{\pi x} \sum_{k=1}^{\infty} \frac{\Gamma(\frac{2k}{\alpha} + 1)}{k!} \left(\frac{\rho}{x^{\frac{2}{\alpha}}}\right)^k \sin k\pi(1 - \frac{2}{\alpha}), \quad (20)$$

where $\Gamma(\cdot)$ is the gamma function.

Proof: We define a new auxiliary variable $\epsilon_0 \to 0^+$. By employing the techniques of Laplace Transform and Cauchy Integral Theorem, $f_{V_{W_j}}(x)$ in (20) is calculated as

$$\begin{aligned}
&f_{V_{W_j}}(x) = \mathcal{L}^{-1}_{V_{W_j}}(s) \\
&= \sum_{k=0}^{\infty}(-1)^k \frac{\rho^k}{k!} \int_{0^+-\infty \mathrm{i}}^{0^+-\infty \mathrm{i}} s^{\frac{2k}{\alpha}} e^{xs} \frac{ds}{2\pi \mathrm{i}} \\
&= \sum_{k=0}^{\infty}(-1)^k \frac{\rho^k}{k!} \Bigg(- \int_{-\infty}^{-\epsilon_0} (-s)^{\frac{2k}{\alpha}} \mathrm{e}^{\frac{2k\pi \mathrm{i}}{\alpha}} \mathrm{e}^{xs} \frac{ds}{2\pi \mathrm{i}} - \frac{\epsilon_0^{\frac{2k}{\alpha}+1} \sin(\frac{2k\pi}{\alpha})}{\left(\frac{2k}{\alpha}+1\right)\pi} \\
&\quad - \int_{-\epsilon_0}^{-\infty} (-s)^{\frac{2k}{\alpha}} \mathrm{e}^{-\frac{2k\pi \mathrm{i}}{\alpha}} \mathrm{e}^{xs} \frac{ds}{2\pi \mathrm{i}} \Bigg) \\
&= \sum_{k=0}^{\infty}(-1)^k \frac{\rho^k}{k!} \Bigg(- \mathrm{e}^{\frac{2k\pi \mathrm{i}}{\alpha}} \int_{\epsilon_0}^{\infty} s^{\frac{2k}{\alpha}} \mathrm{e}^{-xs} \frac{ds}{2\pi \mathrm{i}} - \frac{\epsilon_0^{\frac{2k}{\alpha}+1} \sin(\frac{2k\pi}{\alpha})}{\left(\frac{2k}{\alpha}+1\right)\pi} \\
&\quad + \mathrm{e}^{-\frac{2k\pi \mathrm{i}}{\alpha}} \int_{\epsilon_0}^{\infty} s^{\frac{2k}{\alpha}} \mathrm{e}^{-xs} \frac{ds}{2\pi \mathrm{i}} \Bigg) \\
&= \sum_{k=0}^{\infty}(-1)^k \frac{\rho^k}{k!} \Bigg(- \frac{\epsilon_0^{\frac{2k}{\alpha}+1} \sin(\frac{2k\pi}{\alpha})}{\left(\frac{2k}{\alpha}+1\right)\pi} \\
&\quad - \frac{\sin(\frac{2k\pi}{\alpha})}{\pi} \int_{\epsilon_0}^{\infty} s^{\frac{2k}{\alpha}} \mathrm{e}^{-xs} ds \Bigg),
\end{aligned} \tag{21}$$

where $\mathcal{L}^{-1}_{V_{W_j}}(s)$ is the inverse Laplace transform of $\mathcal{L}_{V_{W_j}}(s)$. Substituting $\epsilon_0 \to 0^+$ into (21) complete the proof. ■

Thus, the CDF $\mathcal{F}_{V_{W_j}}(x)$ of V_{W_j} is given by

$$\mathcal{F}_{V_{W_j}}(x) = 1 - \frac{1}{\pi} \sum_{k=1}^{\infty} \frac{\Gamma(\frac{2k}{\alpha})}{k!} \left(\frac{\rho}{x^{\frac{2}{\alpha}}}\right)^k \sin k\pi(1-\frac{2}{\alpha}). \tag{22}$$

Let $V_Z = \sum_{v=1}^{m} V_{W_v}$ denote the aggregate interference power at W_Z. Following the same procedure in Lemma 1, we can calculate the PDF of V_Z in the following proposition.

Proposition 1: The PDF $f_{V_Z}(x)$ of the total aggregate interference V_Z at W_Z is given by

$$f_{V_Z}(x) = \frac{1}{\pi x} \sum_{k=1}^{\infty} \frac{\Gamma(\frac{2k}{\alpha}+1)}{k!} \left(\frac{m\rho}{x^{\frac{2}{\alpha}}}\right)^k \sin k\pi(1-\frac{2}{\alpha}). \tag{23}$$

Proof: Note that the PDF $f_{V_{W_v}}(x)$ shares the same form as $f_{V_{W_j}}(x)$. The Laplace transform of V_Z evaluated at s can be determined by the convolution property of Laplace transform as

$$\mathcal{L}_{V_Z}(s) = e^{-m\rho s^{\frac{2}{\alpha}}}. \tag{24}$$

The PDF of V_Z can be obtained by taking the inverse Laplace transform of $\mathcal{L}_{V_Z}(s)$, that is,

$$f_{V_Z}(x) = \mathcal{L}^{-1}_{V_Z}(s). \tag{25}$$

By replacing the term $\frac{\rho}{x^{\frac{2}{\alpha}}}$ in (20) with $\frac{m\rho}{x^{\frac{2}{\alpha}}}$, we have (23). ■

This further yields

$$\mathcal{F}_{V_Z}(x) = 1 - \frac{1}{\pi} \sum_{k=1}^{\infty} \frac{\Gamma(\frac{2k}{\alpha})}{k!} \left(\frac{m\rho}{x^{\frac{2}{\alpha}}}\right)^k \sin k\pi(1-\frac{2}{\alpha}). \tag{26}$$

B. Covert Outage Probability

Based on the correct detection probability p_{W_j} in (10), we rewrite the covert outage probability $\mathcal{P}_{cov}$ in (15) as

$$\begin{aligned}
\mathcal{P}_{cov} &= 1 - \mathbb{P}\left\{ \bigcap_{j=m+1}^{M} p_{W_j} = \frac{1}{2} \quad \text{and} \quad p_Z = \frac{1}{2} \right\} \\
&= 1 - \prod_{j=m+1}^{M} \left(1 - \tilde{p}_{W_j}\right)\left(1 - \tilde{p}_Z\right),
\end{aligned} \tag{27}$$

where $\tilde{p}_{W_j} = \mathbb{P}\{p_{W_j} = 1\}$ and $\tilde{p}_Z = \mathbb{P}\{p_Z = 1\}$ denote the average detection probabilities at W_j and W_Z, respectively. In what follows, $\tilde{p}_{W_j}$ and $\tilde{p}_Z$ are calculated step by step.

1) Average detection probability $\tilde{p}_{W_j}$ at W_j: Revisit expression (10), we have

$$\begin{aligned}
\tilde{p}_{W_j} &= \mathbb{P}\{p_{W_j} = 1\} = \mathbb{P}\{V_{W_j} \le \xi_1 < U_{W_j} + V_{W_j}\} \\
&\overset{(a)}{=} \mathbb{P}\{\xi_1 - P_A d_{A,W_j}^{-\alpha} < V_{W_j} \le \xi_1\},
\end{aligned} \tag{28}$$

where (a) is due to $U_{W_j} = P_A d_{A,W_j}$.

According to (22) and (28), the average detection probability $\tilde{p}_{W_j}$ at W_j is given by

$$\begin{aligned}
\tilde{p}_{W_j} =& \frac{1}{\pi} \sum_{k=1}^{\infty} \frac{\Gamma(\frac{2k}{\alpha})}{k!} \left(\frac{\rho^k}{\left(\xi_1 - P_A d_{A,W_j}^{-\alpha}\right)^{\frac{2k}{\alpha}}} - \frac{\rho^k}{\xi_1^{\frac{2k}{\alpha}}} \right) \\
& \sin k\pi(1-\frac{2}{\alpha}).
\end{aligned} \tag{29}$$

2) Average detection probability $\tilde{p}_Z$ at W_Z: Similar to expression (28), the average detection probability $\tilde{p}_Z$ can be reformulated as

$$\begin{aligned}
\tilde{p}_Z =& \mathbb{P}\{p_Z = 1\} = \mathbb{P}\{V_Z \le \xi_2 < U_Z + V_Z\} \\
=& \mathbb{P}\left\{ \xi_2 - \sum_{v=1}^{m} P_A d_{A,W_v}^{-\alpha} < V_Z \le \xi_2 \right\},
\end{aligned} \tag{30}$$

where $U_Z = \sum_{v=1}^{m} U_{W_v}$.

From (26), the average detection probability $\tilde{p}_Z$ at W_Z is given by

$$\begin{aligned}
\tilde{p}_Z =& \frac{1}{\pi} \sum_{k=1}^{\infty} \frac{\Gamma(\frac{2k}{\alpha})}{k!} \left(\frac{m^k \rho^k}{\left(\xi_2 - \sum_{v=1}^{m} P_A d_{A,W_v}^{-\alpha}\right)^{\frac{2k}{\alpha}}} - \frac{m^k \rho^k}{\xi_2^{\frac{2k}{\alpha}}} \right) \\
& \sin k\pi(1-\frac{2}{\alpha}).
\end{aligned} \tag{31}$$

Substituting (29) and (31) into (27), we finally derive the covert outage probability for the covert communication under AWGN channels as (32), shown at the top of the next page.

C. Connection Outage Probability

Based on the expression (17), we rewrite the connection outage probability $\mathcal{P}_{con}$ as

$$\begin{aligned}
\mathcal{P}_{con} &= \mathbb{P}\left\{ V_B > \frac{U_B}{\beta} \right\} = 1 - \mathbb{P}\left\{ V_B \le \frac{N_A P_A d_{A,B}^{-\alpha}}{\beta} \right\} \\
&= 1 - \mathcal{F}_{V_B}\left(\frac{N_A P_A d_{A,B}^{-\alpha}}{\beta} \right).
\end{aligned} \tag{33}$$

$$\mathcal{P}_{cov}=1-\prod_{j=m+1}^{M}\left(1-\frac{1}{\pi}\sum_{k=1}^{\infty}\frac{\Gamma(\frac{2k}{\alpha})}{k!}\left(\frac{\rho^k}{(\xi_1-P_Ad_{A,W_j}^{-\alpha})^{\frac{2k}{\alpha}}}-\frac{\rho^k}{\xi_1^{\frac{2k}{\alpha}}}\right)\sin k\pi(1-\frac{2}{\alpha})\right)$$
$$\left(1-\frac{1}{\pi}\sum_{k=1}^{\infty}\frac{\Gamma(\frac{2k}{\alpha})}{k!}\left(\frac{m^k\rho^k}{(\xi_2-\sum_{v=1}^{m}P_Ad_{A,W_v}^{-\alpha})^{\frac{2k}{\alpha}}}-\frac{m^k\rho^k}{\xi_2^{\frac{2k}{\alpha}}}\right)\sin k\pi(1-\frac{2}{\alpha})\right) \quad (32)$$

Note that the CDF $\mathcal{F}_{V_B}(x)$ has the same form as (22). Thus, we have

$$\mathcal{P}_{con}=\frac{1}{\pi}\sum_{k=1}^{\infty}\frac{\Gamma(\frac{2k}{\alpha})}{k!}\left(\frac{\rho}{(N_AP_Ad_{A,B}^{-\alpha}\beta^{-1})^{\frac{2}{\alpha}}}\right)^k\sin k\pi(1-\frac{2}{\alpha}). \quad (34)$$

D. Covert Throughput

From expressions (18), (32) and (34), we can see that the predefined transmit power P_A and transmission rate R will determine the covert throughput of the system. In this subsection, we aim to explore the joint design of P_A and R for covert throughput optimization problem to illustrate the impact of warden collusion. The optimization problem can be mathematically formulated as follows:

$$\max_{P_A,R} \quad \eta=(1-\mathcal{P}_{con})R \quad (35a)$$
$$\text{s.t.} \quad \mathcal{P}_{cov}\le\epsilon. \quad (35b)$$

Note that $\mathcal{P}_{con}$ is a function of both P_A and R but $\mathcal{P}_{cov}$ is function of only P_A. Thus, problem (35) can be equivalently transformed into

$$\max_{P_A,R} \quad \eta=\max_{R}\left(\max_{P_A}(1-\mathcal{P}_{con})R\right) \quad (36a)$$
$$\text{s.t.} \quad \mathcal{P}_{cov}\le\epsilon. \quad (36b)$$

To solve (36), we can first maximize $(1-\mathcal{P}_{con})$ over P_A with constraint $\mathcal{P}_{cov}\le\epsilon$ and a fixed R, and then maximize $(1-\mathcal{P}_{con})R$ over R. The optimization procedure is performed as follows.

1) Optimal P_A^*: Before calculating the optimal P_A^*, we give the following proposition to reveal the monotonicity of $\mathcal{P}_{cov}$ and $\mathcal{P}_{con}$ with respect to P_A.

Proposition 2: The values of $(1-\mathcal{P}_{con})$ and $\mathcal{P}_{cov}$ monotonically increase with P_A.

Proof: We consider two different source's transmit power $P_{A,1}$ and $P_{A,2}$ with $P_{A,1}<P_{A,2}$. It is observed from (33) that when P_A increases, the feasible region $\{V_B>\frac{N_AP_Ad_{A,B}^{-\alpha}}{\beta}\}$ of V_B is narrowed. Thus, we have $\mathcal{P}_{con}(P_{A,1})>\mathcal{P}_{con}(P_{A,2})$, i.e., $1-\mathcal{P}_{con}(P_{A,1})<1-\mathcal{P}_{con}(P_{A,2})$, where $\mathcal{P}_{con}(P_{A,1})$ and $\mathcal{P}_{con}(P_{A,2})$ are the value of P_{con} at $P_{A,1}$ and $P_{A,2}$, respectively. Similarly, from (27), (29) and (31), it is inferred that $\mathcal{P}_{cov}(P_{A,1})<\mathcal{P}_{cov}(P_{A,2})$. ■

Based on Proposition 1, we note that the optimal solution P_A^* of (36) must satisfy $\mathcal{P}_{cov}(P_A^*)=\epsilon$, where $\mathcal{P}_{cov}(P_A^*)$ is the value of P_{cov} at point $P_A=P_A^*$. Therefore, P_A^* can be efficiently calculated via a bisection search.

2) Optimal R^*: Next, we need to determine the optimal transmission rate R^* that maximizes the covert throughput $\eta=(1-\mathcal{P}_{con}(P_A^*))R$. Since $(1-\mathcal{P}_{con}(P_A^*))$ decreases with R, it is difficult to directly obtain the monotonicity of η with respect to R. Here, we provide the following proposition to claim the concavity of the objective function.

Proposition 3: For the fixed P_A^*, the objective function $(1-\mathcal{P}_{con}(P_A^*))R$ is concave with respect to R.

Proof: To prove this proposition, we first compute the second derivative $\frac{d^2\eta}{dR^2}$, and then prove $\frac{d^2\eta}{dR^2}<0$.

The derivative $\frac{d\eta}{dR}$ can be expressed as

$$\frac{d\eta}{dR}=1-\left(\frac{d\mathcal{P}_{con}}{dR}R+\mathcal{P}_{con}\right)$$
$$=1-\sum_{k=1}^{\infty}\left(\frac{2k\varphi R}{\alpha}(2^R-1)^{\frac{2k}{\alpha}-1}2^R\ln 2+\varphi\left(2^R-1\right)^{\frac{2k}{\alpha}}\right). \quad (37)$$

where

$$\varphi=\frac{1}{\pi}\frac{\Gamma(\frac{2k}{\alpha})}{k!}\left(\frac{\rho}{(P_Ad_{A,B}^{-\alpha})^{\frac{2}{\alpha}}}\right)^k\sin k\pi(1-\frac{2}{\alpha}). \quad (38)$$

Based on expression (37), the second derivative $\frac{d^2\eta}{dR^2}$ is given by

$$\frac{d^2\eta}{dR^2}=-\frac{d^2\mathcal{P}_{con}}{dR^2}R-2\frac{d\mathcal{P}_{con}}{dR}$$
$$=-\sum_{k=1}^{\infty}\varphi\left[\frac{2kR\ln 2}{\alpha}\left(\left(\frac{2k}{\alpha}-1\right)(2^R-1)^{\frac{2k}{\alpha}-2}2^{2R}\ln 2\right.\right.$$
$$\left.\left.+(2^R-1)^{\frac{2k}{\alpha}-1}2^R\ln 2\right)+\frac{4k}{\alpha}(2^R-1)^{\frac{2k}{\alpha}-1}2^R\ln 2\right]$$
$$=-\sum_{k=1}^{\infty}\frac{2k\varphi\ln 2}{\alpha}(2^R-1)^{\frac{2k}{\alpha}-2}2^R$$
$$\left[R(\frac{2k}{\alpha}-1)2^R\ln 2+R(2^R-1)\ln 2+2(2^R-1)\right]$$
$$=-\sum_{k=1}^{\infty}\chi_1\chi_2, \quad (39)$$

where χ_1 and χ_2 are respectively given by

$$\chi_1=\frac{2k\varphi\ln 2}{\alpha}(2^R-1)^{\frac{2k}{\alpha}-2}2^R, \quad (40)$$
$$\chi_2=R(\frac{2k}{\alpha}-1)2^R\ln 2+R(2^R-1)\ln 2+2(2^R-1). \quad (41)$$

Since $R>0$, it is easily seen that χ_1 has the same sign with φ, hence $\sum_{k=1}^{\infty}\chi_1$ has the same sign with the connection outage probability $\mathcal{P}_{con}$, i.e. $\sum_{k=1}^{\infty}\chi_1>0$. Therefore, we only need to determine the sign of χ_2 to prove $\frac{d^2\eta}{dR^2}<0$.

The derivative $\frac{d\chi_2}{dR}$ is given by

$$\frac{d\chi_2}{dR} = 2^{R+1}\ln 2 + \frac{2k\ln 2}{\alpha}(R2^R\ln 2 + 2^R) - \ln 2, \quad (42)$$

which is always large than zero due to $R > 0$. From (42), it is further deduced that $\chi_2 > 0$.

By combining the above analysis, we can conclude that $\frac{d^2\eta}{dR^2} < 0$. This completes the proof. ∎

Proposition 3 indicates that there is only one zero-crossing of $\frac{d\eta}{dR}$, that is, $\frac{d\eta}{dR}|_{R=R^*} = 0$. Therefore, the optimal R^* can be also obtained by using Newton's method.

Formally, we summarize the proposed methodology for solving (35) in Algorithm 1.

Algorithm 1: Covert Throughput Optimization Algorithm

Input: Tolerance ϵ, ε, power bounds P_{min}, P_{max}, maximum number of iterations c_{max}, initial value R_0, initial iteration count $c = 0$;

Output: Optimal P_A^*, R^*, η^*;

while $|P_{max} - P_{min}| > \varepsilon$ **do**
  $P_{mid} = \frac{P_{min}+P_{max}}{2}$;
  $P_{max}, P_{min} = (P_{mid}, P_{min})$ **if** $\mathcal{P}_{cov}(P_{mid}) > \epsilon$ based on (32) **else** (P_{max}, P_{mid});
$P_A^* = P_{min}$;
while $|\frac{d\eta}{dR}(R_0)| \geq \varepsilon$ ***and*** $c < c_{max}$ **do**
  Compute $\frac{d\eta}{dR}(R_0)$ and $\frac{d^2\eta}{dR^2}(R_0)$;
  $R_0 = R_0 - \frac{\frac{d\eta}{dR}(R_0)}{\frac{d^2\eta}{dR^2}(R_0)}$;
  $c = c + 1$;
$R^* = R_0$;
$\eta^* = (1 - \mathcal{P}_{con}(P_A^*)) \cdot R^*$;
return P_A^*, R^*, η^*;

IV. Warden Collusion Under Rayleigh Fading Channel

In this section, we investigate the impact of warden collusion on the covert communication in Rayleigh fading channels, where $h_{I_y,B}$, h_{I_y,W_j}, h_{I_y,W_v} and the elements of $\mathbf{h}_{A,B}$, $\mathbf{h}_{A,W_j}$, and $\mathbf{h}_{A,W_v}$ are independent and identically distributed (i.i.d.) with zero mean and unit variance.

A. Aggregate Interference Distribution

Recalling the Lemma 1 in Section III, the PDF $f_{V_{W_j}}(x)$ in Rayleigh fading channels can be reformulated as

$$\begin{aligned} f_{V_{W_j}}(x) =& \frac{1}{\pi x}\sum_{k=1}^{\infty}\frac{(-1)^{k+1}\Gamma(\frac{2k}{\alpha}+1)}{k!}\sin\left(\frac{2k\pi}{\alpha}\right) \\ & \left(\frac{\rho\mathbb{E}\{|h_{I_y,W_j}|^{\frac{4}{\alpha}}\}}{x^{\frac{2}{\alpha}}}\right)^k \\ \overset{(b)}{=}& \frac{1}{\pi x}\sum_{k=1}^{\infty}\frac{(-1)^{k+1}\Gamma(\frac{2k}{\alpha}+1)}{k!}\sin\left(\frac{2k\pi}{\alpha}\right) \\ & \left(\frac{\rho\Gamma(1+\frac{2}{\alpha})}{x^{\frac{2}{\alpha}}}\right)^k, \end{aligned} \quad (43)$$

where (b) is due to $\mathbb{E}\{|h_{I_y,W_j}|^{\frac{4}{\alpha}}\} = \Gamma(1+\frac{2}{\alpha})$ in Rayleigh fading case. Accordingly, the CDF $\mathcal{F}_{V_{W_j}}(x)$ can be formulated as

$$\begin{aligned} \mathcal{F}_{V_{W_j}}(x) =& 1 - \frac{1}{\pi}\sum_{k=1}^{\infty}\frac{(-1)^{k+1}\Gamma(\frac{2k}{\alpha})}{k!}\sin\left(\frac{2k\pi}{\alpha}\right) \\ & \left(\frac{\rho\Gamma(1+\frac{2}{\alpha})}{x^{\frac{2}{\alpha}}}\right)^k. \end{aligned} \quad (44)$$

By combining the expressions (19), (24), (26) and (44), we further derive the CDF $\mathcal{F}_{V_Z}(x)$ as

$$\begin{aligned} \mathcal{F}_{V_Z}(x) =& 1 - \frac{1}{\pi}\sum_{k=1}^{\infty}\frac{(-1)^{k+1}\Gamma(\frac{2k}{\alpha})}{k!}\sin\left(\frac{2k\pi}{\alpha}\right) \\ & \left(\frac{m\rho\Gamma(1+\frac{2}{\alpha})}{x^{\frac{2}{\alpha}}}\right)^k. \end{aligned} \quad (45)$$

B. Covert Outage Probability

1) Average detection probability $\tilde{p}_{W_j}$ at W_j: From expression (10), we have

$$\begin{aligned} \tilde{p}_{W_j} =& \mathbb{P}\left\{V_{W_j} \leq \xi_1 < U_{W_j} + V_{W_j}\right\} \\ =& \mathbb{P}\left\{V_{W_j} \leq \xi_1\right\}\mathbb{P}\left\{U_{W_j} > \xi_1 - V_{W_j} | V_{W_j} \leq \xi_1\right\} \\ =& \mathcal{F}_{V_{W_j}}(\xi_1) - \mathcal{F}_{U_{W_j}+V_{W_j}}(\xi_1) \\ =& \mathcal{F}_{V_{W_j}}(\xi_1) - \int_0^{\xi_1}\mathcal{F}_{V_{W_j}}(\xi_1 - x) f_{U_{W_j}}(x)\,dx. \end{aligned} \quad (46)$$

It is notable in (29) that U_{W_j} is an exponentially distributed random variable with mean $\theta = P_A d_{A,W_j}^{-\alpha}$, and thus the PDF of U_{W_j} can be expressed as

$$f_{U_{W_j}}(x) = \frac{1}{\theta}e^{-\frac{x}{\theta}}. \quad (47)$$

Equations (44) and (47) make it complicated to analyze $\tilde{p}_{W_j}$. In order to circumvent such a difficulty and facilitate the subsequent solution of $\mathcal{P}_{cov}$, we consider a practical scenario with high path loss α. In particular, by concentrating on the high path loss regime, we derive a simplified expression for $\tilde{p}_{W_j}$, as detailed in the following proposition.

Proposition 4: For the high path loss regime, the average detection probability $\tilde{p}_{W_j}$ at W_j is approximated by

$$\tilde{p}_{W_j} \approx e^{-\frac{\xi_1}{\theta}} + \frac{1}{\pi}\sum_{k=1}^{L}\psi(k)(1 - e^{-\frac{\xi_1}{\theta}} - \xi_1^{-\frac{2k}{\alpha}}), \quad (48)$$

where

$$\psi(k) = \frac{(-1)^{k+1}\Gamma(\frac{2k}{\alpha})\sin\left(\frac{2k\pi}{\alpha}\right)}{k!}\rho^k\Gamma\left(1+\frac{2}{\alpha}\right)^k \quad (49)$$

and L is the number of terms applied for the approximation.

Proof: Substituting (44) and (47) and (46), we have

$$\begin{aligned} \tilde{p}_{W_j} =& 1 - \frac{1}{\pi}\sum_{k=1}^{\infty}\frac{(-1)^{k+1}\Gamma(\frac{2k}{\alpha})}{k!}\sin\left(\frac{2k\pi}{\alpha}\right)\left(\frac{\rho\Gamma(1+\frac{2}{\alpha})}{\xi_1^{\frac{2}{\alpha}}}\right)^k \\ & - \int_0^{\xi_1}\left(1 - \frac{1}{\pi}\sum_{k=1}^{\infty}\frac{(-1)^{k+1}\Gamma(\frac{2k}{\alpha})}{k!}\sin\left(\frac{2k\pi}{\alpha}\right)\right. \\ & \left.\left(\frac{\rho\Gamma(1+\frac{2}{\alpha})}{(\xi_1 - x)^{\frac{2}{\alpha}}}\right)^k\right)\left(\frac{1}{\theta}e^{-\frac{x}{\theta}}\right)dx. \end{aligned} \quad (50)$$

Then, the result can be follow easily by considering $\frac{2}{\alpha} \to 0$ in (50). ∎

2) Average detection probability $\tilde{p}_Z$ at W_Z: Similarly, according to expression (11), the average detection probability $\tilde{p}_Z$ at W_Z is given by

$$\begin{aligned}\tilde{p}_Z =&\mathbb{P}\left\{V_Z \le \xi_2 < U_Z + V_Z\right\}\\ =&\mathcal{F}_{V_Z}(\xi_2) - \int_0^{\xi_2} \mathcal{F}_{V_Z}(\xi_2 - x) f_{U_Z}(x)\, dx. \end{aligned} \tag{51}$$

Next, we can derive the PDF $f_{U_Z}(x)$ by using the following lemma and theorem.

Lemma 2: Define $\mu_v = P_A^{-1} d_{A,W_v}^{\alpha}$, the following equality always holds:

$$\begin{aligned}(-1)^{m-2}\frac{1}{\prod_{\tau=1}^{m-1}(\mu_m - \mu_\tau)} =& \frac{1}{\prod_{v=2}^{m}(\mu_v - \mu_1)}\\ -& \frac{1}{\prod_{v=3}^{m}(\mu_v - \mu_2)(\mu_2 - \mu_1)} + ...\\ +& (-1)^{m-2}\frac{1}{\prod_{v=m}^{m}(\mu_v - \mu_{m-1})\prod_{\tau=1}^{m-2}(\mu_{m-1} - \mu_\tau)}. \end{aligned} \tag{52}$$

Proof: Please refer to Appendix A. ∎

Theorem 1: The PDF $f_{U_Z}(x)$ in (31) can be expressed as

$$\begin{aligned}f_{U_Z}(x) =& \prod_{v=1}^{m}\mu_v \left(\frac{e^{-\mu_1 x}}{\prod_{v=2}^{m}(\mu_v - \mu_1)} - \frac{e^{-\mu_2 x}}{\prod_{v=3}^{m}(\mu_v - \mu_2)(\mu_2 - \mu_1)}\right.\\ &\left. + ... + (-1)^{m-1}\frac{e^{-\mu_m x}}{\prod_{\tau=1}^{m-1}(\mu_m - \mu_\tau)}\right). \end{aligned} \tag{53}$$

Proof: Please refer to Appendix B. ∎

Similar to the analysis with respect to $\tilde{p}_{W_j}$, in the following proposition, we provide the expression of $\tilde{p}_Z$ under the high path loss regime.

Proposition 5: For the high path loss regime, the average detection probability $\tilde{p}_Z$ at W_Z is approximated by

$$\tilde{p}_Z \approx 1 - \Theta + \frac{1}{\pi}\sum_{k=1}^{L}\psi(k) m^k \left(\Theta - \xi_2^{-\frac{2k}{\alpha}}\right), \tag{54}$$

where

$$\begin{aligned}\Theta = \prod_{v=1}^{m}\mu_v \left(\frac{\mu_1^{-1}(1 - e^{-\mu_1\xi_2})}{\prod_{v=2}^{m}(\mu_v - \mu_1)} - \frac{\mu_2^{-1}(1 - e^{-\mu_2\xi_2})}{\prod_{v=3}^{m}(\mu_v - \mu_2)(\mu_2 - \mu_1)}\right.\\ \left. + ... + (-1)^{m-1}\frac{\mu_m^{-1}(1 - e^{-\mu_m\xi_2})}{\prod_{\tau=1}^{m-1}(\mu_m - \mu_\tau)}\right). \end{aligned} \tag{55}$$

Proof: Let $\frac{2}{\alpha} \to 0$, and substituting (53) and (45) into (51) yields (54). ∎

Having obtained $\tilde{p}_{W_j}$ and $\tilde{p}_Z$, the covert outage probability for the covert communication under Rayleigh fading channels is calculated as

$$\begin{aligned}\mathcal{P}_{cov} \approx 1 - \prod_{j=m+1}^{M}&\left(1 - e^{-\frac{\xi_1}{\theta}} - \frac{1}{\pi}\sum_{k=1}^{L}\psi(k)(1 - e^{-\frac{\xi_1}{\theta}}\right.\\ &\left. - \xi_1^{-\frac{2k}{\alpha}})\right)\left(\Theta - \frac{1}{\pi}\sum_{k=1}^{L}\psi(k) m^k\left(\Theta - \xi_2^{-\frac{2k}{\alpha}}\right)\right). \end{aligned} \tag{56}$$

C. Connection Outage Probability

Theorem 2: The connection outage probability $\mathcal{P}_{con}$ is given by

$$\begin{aligned}\mathcal{P}_{con} = 1 - \Bigg(&e^{-\rho\Gamma(1+\frac{2}{\alpha})\zeta^{\frac{2}{\alpha}}} + e^{-\rho\Gamma(1+\frac{2}{\alpha})\zeta^{\frac{2}{\alpha}}}\sum_{k=1}^{N_A-1}\frac{1}{k!}\\ &\sum_{l=1}^{k}\Big(\frac{2\rho\Gamma(1+\frac{2}{\alpha})\zeta^{\frac{2}{\alpha}}}{\alpha}\Big)^l \Upsilon_{k,l}\Bigg), \end{aligned} \tag{57}$$

where

$$\Upsilon_{k,l} = \sum_{\gamma_b \in \mathrm{comb}\binom{k-1}{k-l}}\prod_{c_{ab}\in\gamma_b}\left(c_{ab} - \frac{2}{\alpha}(c_{ab} - a + 1)\right), \tag{58}$$

comb denotes the set of all distinct subsets γ_b of the natural numbers $\{1, 2, \cdots, k-1\}$ with cardinality $k-l$. The elements in each subset are arranged in an ascending order with c_{ab} being the a-th element of γ_b. For $k \ge 1$, it is set $\Upsilon_{k,k} = 1$.

Proof: Based on the expression (17), we rewrite the connection outage probability $\mathcal{P}_{con}$ as

$$\begin{aligned}\mathcal{P}_{con} &= \mathbb{E}_{V_B}\left[\mathbb{P}\left\{U_B < \beta V_B\right\}\right]\\ &= \mathbb{E}_{V_B}\left[\mathbb{P}\left\{||\mathbf{h}_{A,B}||^2 < P_A^{-1} d_{A,B}^{\alpha}\beta V_B\right\}\right]\\ &= \mathbb{E}_{V_B}\left[\mathbb{P}\left\{||\mathbf{h}_{A,B}||^2 < \zeta V_B\right\}\right], \end{aligned} \tag{59}$$

where $\zeta = P_A^{-1} d_{A,B}^{\alpha}\beta$. Since $||\mathbf{h}_{A,B}||^2$ is a normalized gamma random variable with the shape parameter N_A, $\mathcal{P}_{con}$ can be calculated as follows:

$$\begin{aligned}\mathcal{P}_{con} &= 1 - \mathbb{E}_{V_B}\left[e^{-\zeta V_B}\sum_{k=0}^{N_A-1}\frac{(\zeta V_B)^k}{k!}\right]\\ &= 1 - \sum_{k=0}^{N_A-1}\frac{\zeta^k}{k!}\mathbb{E}_{V_B}\left[V_B^k e^{-\zeta V_B}\right]\\ &\overset{(c)}{=} 1 - \sum_{k=0}^{N_A-1}\frac{(-\zeta)^k}{k!}\cdot\mathcal{L}_{V_B}^{(k)}(\zeta), \end{aligned} \tag{60}$$

where $\mathcal{L}_{V_B}(\zeta)$ is the Laplace transform of V_B evaluated at ζ, i.e. $\mathcal{L}_{V_B}(\zeta) = e^{-\rho\Gamma(1+\frac{2}{\alpha})\zeta^{\frac{2}{\alpha}}}$, $\mathcal{L}_{V_B}^{(k)}(\zeta)$ is the k-th derivative of $\mathcal{L}_{V_B}(\zeta)$, and (c) is due to $(-1)^k\mathcal{L}_{V_B}^{(k)}(\zeta) = \mathbb{E}_{V_B}\left[V_B^k e^{-\zeta V_B}\right]$. By simplifying (60), we complete the proof. ∎

D. Covert Throughput

The covert throughput optimization problem can be formulated similarly to (35 and can be resolved by executing the same two-step process for the AWGN channel described in Section III-C.

In this case, the optimal solution P_A^* also satisfy $\mathcal{P}_{cov}(P_A^*) = \epsilon$, which can be obtained by using bisection search method. Thus, the problem is transformed into

$$\max_{R} \quad \eta = (1 - \mathcal{P}_{con})R. \tag{61}$$

Due to the complicated expression of $\mathcal{P}_{con}$ in (57), it is difficult to prove the monotonicity of η with respect to R. To circumvent this issue, we consider a high reliability scenario and propose an approximate solution to problem

(61). Particularly, in scenarios where the connection outage probability P_{con} approaches zero, the subsequent lemma offers a concise expression for P_{con}.

Lemma 3: In the high reliability regime $P_{con} \to 0$, P_{con} in (57) is approximated by

$$\mathcal{P}_{con} \approx 1 - e^{-\hat{\rho}\zeta^{\frac{2}{\alpha}}} - \kappa\hat{\rho}\zeta^{\frac{2}{\alpha}} e^{-\hat{\rho}\zeta^{\frac{2}{\alpha}}}, \tag{62}$$

where $\kappa = \sum_{k=1}^{N_A-1} \frac{2\Upsilon_{k,1}}{\alpha k!}$ and $\hat{\rho} = \rho\Gamma(1+\frac{2}{\alpha})$.

Proof: As ρ approaches 0, $\mathcal{P}_{con}$ tends to 0. Discarding the high-order terms in (57) yields (62). ∎

Note that $\zeta = P_A^{-1} d_{A,B}^{\alpha}(2^R - 1)$ monotonically increases with R. Based on Lemma 3, problem (61) can be equivalently transformed into

$$\max_{\zeta} \quad \eta = \ln\left(1 + \frac{P_A\zeta}{d_{A,B}^{\alpha}}\right)\left(1 + \kappa\hat{\rho}\zeta^{\frac{2}{\alpha}}\right) e^{-\hat{\rho}\zeta^{\frac{2}{\alpha}}}. \tag{63}$$

Subsequently, the solution to (63) is provided by the following theorem.

Theorem 3: The objective function η in equation (63) initially increases and then decreases as ζ changes, and the optimal ζ^* is the unique root of $\zeta > 0$ satisfying the equation

$$Y(\zeta) = \frac{P_A(1+\kappa\hat{\rho}\zeta^{\frac{2}{\alpha}})}{d_{A,B}^{\alpha}(1+\frac{P_A\zeta}{d_{A,B}^{\alpha}})} + \frac{2\hat{\rho}\zeta^{\frac{2}{\alpha}-1}\ln\left(1+\frac{P_A\zeta}{d_{A,B}^{\alpha}}\right)}{\alpha(\kappa - 1 - \kappa\hat{\rho}\zeta^{\frac{2}{\alpha}})^{-1}} = 0. \tag{64}$$

Proof: The derivative of objective function (63) with respect to ζ is given by $\frac{d\eta}{d\zeta} = Y(\zeta)e^{-\hat{\rho}\zeta^{\frac{2}{\alpha}}}$. It is verified easily that $\frac{d\eta}{d\zeta}|_{\zeta=0} = 1$ and $\frac{d\eta}{d\zeta}|_{\zeta\to\infty} < 0$. This implies there is at least one zero-crossing of $\frac{d\eta}{d\zeta}$. When $\frac{d\eta}{d\zeta}|_{\zeta=\zeta^*} = 0$, we have $Y(\zeta^*)$=0.

Taking the second derivative of η with respect to ζ^*, we have

$$\begin{aligned}
\frac{d^2\eta}{d\zeta^2}|_{\zeta=\zeta^*} &= e^{-\hat{\rho}\zeta^{\frac{2}{\alpha}}}\frac{dY(\zeta)}{d\zeta}|_{\zeta=\zeta^*} \\
&= -\frac{P_A^2 d_{A,B}^{-2\alpha}(\kappa\hat{\rho}\zeta^{\frac{2}{\alpha}}+1)}{(P_A d_{A,B}^{-\alpha}\zeta+1)^2} + \frac{2P_A d_{A,B}^{-\alpha}\kappa\hat{\rho}\zeta^{\frac{2}{\alpha}}}{\alpha\zeta(P_A d_{A,B}^{-\alpha}\zeta+1)} \\
&- \frac{2\hat{\rho}P_A\alpha\zeta^{\frac{2}{\alpha}}(\kappa\hat{\rho}\zeta^{\frac{2}{\alpha}}-\kappa+1)}{\alpha^2\zeta(P_A\zeta+d_{A,B}^{\alpha})} - \frac{4\kappa\hat{\rho}^2\zeta^{\frac{4-\alpha}{\alpha}}\ln\left(\frac{P_A\zeta+d_{A,B}^{\alpha}}{d_{A,B}^{\alpha}}\right)}{\alpha^2\zeta} \\
&+ \frac{2\hat{\rho}\zeta^{\frac{2-\alpha}{\alpha}}(\alpha-2)(\kappa\hat{\rho}\zeta^{\frac{2}{\alpha}}-\kappa+1)\ln\left(\frac{P_A\zeta+d_{A,B}^{\alpha}}{d_{A,B}^{\alpha}}\right)}{\alpha^2\zeta}.
\end{aligned} \tag{65}$$

From (64), we can deduce $\frac{d^2\eta}{d\zeta^2}|_{\zeta=\zeta^*} < 0$. Based on the above analysis, we can conclude that η increases with ζ up to a threshold ζ^*, beyond which it decreases. This completes the proof. ∎

The function $Y(\zeta)$, defined in (64), transitions from positive to negative as ζ increases from zero to infinity. This shift allows for the efficient determination of the optimum using the bisection method based on the condition $Y(\zeta) = 0$, thereby providing a significant time-saving method compared to exhaustive search ones. Once the optimal value of ζ is fixed, we can use the $R = \log_2\left(1 + \frac{P_A\zeta}{d_{A,B}^{\alpha}}\right)$ to obtain the solution of R for problem (61).

Note that by replacing (32) with (56), the value of P_A^* can be obtained by using the same procedure as described in Algorithm 1. Next, we summarize the optimization algorithm for finding R^* in Algorithm 2.

Algorithm 2: Algorithm for Solving Problem (61)

Input: Initial ζ bounds ζ_{min}, ζ_{max}, tolerance ε;
Output: Optimal rate R^*;
while $|\zeta_{max} - \zeta_{min}| > \varepsilon$ **do**
  $\zeta_{mid} = \frac{\zeta_{min}+\zeta_{max}}{2}$;
  $\zeta_{min}, \zeta_{max} = (\zeta_{mid}, \zeta_{max})$ **if** $Y(\zeta_{mid}) > 0$ based on (64) **else** $(\zeta_{min}, \zeta_{mid})$;
$\zeta^* = \zeta_{mid}$;
$R^* = \log_2\left(1 + \frac{P_A\zeta^*}{d_{A,B}^{\alpha}}\right)$;
return R^*;

V. Numerical Results

In this section, we present extensive numerical results to illustrate the impact of warden collusion on the covert communication performance under both the AWGN and Rayleigh channels. For the result of Rayleigh channel, the elements of all channels are independent and identically distributed as complex Gaussian random variables with zero mean and unit variance. Unless otherwise stated, we set the total number of wardens as $M = 10$, the distance between Alice and Bob as $d_{A,B} = 2$, the covertness requirement threshold as $\epsilon = 0.1$. The predefined detection thresholds are set to be $\xi_1 = 1$ and $\xi_2 = 2$, respectively.

A. Model Validation

We plot Figs. 2-4 to compare our theoretical results with simulation results under the AWGN and Rayleigh channels, where we set $\alpha = 4$, $R = 1$ bits/s/Hz, $P_A = 1$ W, $P_I = 1$ W and $N_A = 2$. For each task of simulation, we use 10^6 independent realizations for the Rayleigh fading channels. Without loss of generality, we deploy Alice at the location $\mathbb{L}_A = (0, 0)$. The wardens W_x $(x \in 1, 2, \ldots, M)$ are randomly placed within a square area of size 10^2 centered at $\mathbb{L}_A$, and their locations $\mathbb{L}_{W_x}$ follow a static uniform distribution. The interferers are randomly placed at a sufficiently large square area with an area of 200^2 centered on $\mathbb{L}_A$, and the distribution of their locations follows a homogeneous Poisson point process with density λ.

Under AWGN channels, Fig. 2(a) illustrates the variation of covert outage probability P_{cov} with interferer density λ for different settings of M and m, while Fig. 2(b) shows the variation of connection outage probability P_{con} with λ for different settings of $d_{A,B}$. We can see from both Fig. 2(a) and Fig. 2(b) that the simulation results match well with the theoretical ones for various settings of M, m, and $d_{A,B}$, indicating that our theoretical models under AWGN channels are accurate in capturing the overall performance of the network under such channels.

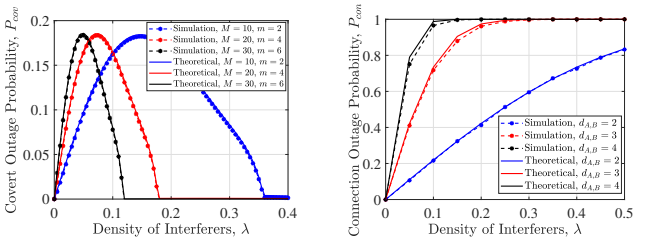

(a) (b)

Fig. 2. Theoretical results validation under the AWGN channels. $\alpha = 4$, $R = 1$ bits/s/Hz, $P_A = 1$ W, $P_I = 1$ W and $N_A = 2$.

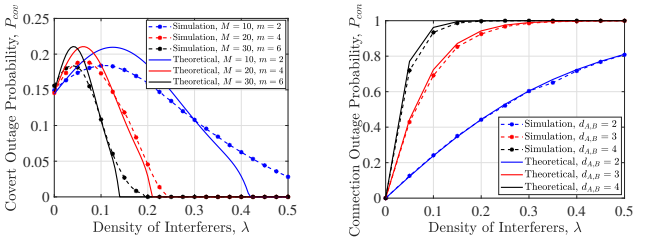

(a) (b)

Fig. 3. Theoretical results validation under the Rayleigh channels. $\alpha = 4$, $R = 1$ bits/s/Hz, $P_A = 1$ W, $P_I = 1$ W and $N_A = 2$.

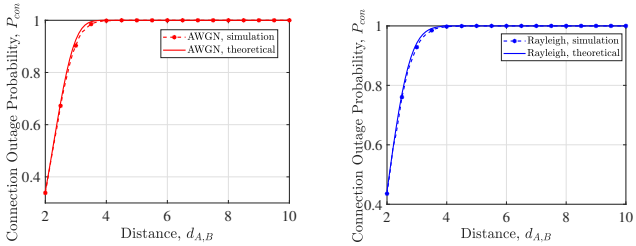

(a) (b)

Fig. 4. Theoretical validation of connection outage probability with varying distance d_{so}. $\lambda = 0.16$, $\alpha = 4$, $R = 1$ bits/s/Hz, $P_A = 1$ W, $P_I = 1$ W and $N_A = 2$.

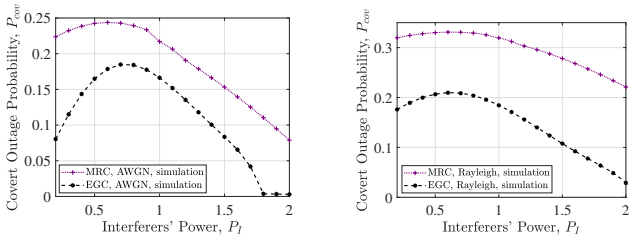

(a) (b)

Fig. 5. Performance comparison of EGC and MRC under the variation of the interferers' power P_I. $m = 2$, $\lambda = 0.2$, $\alpha = 4$, $P_A = 1$ W and $N_A = 2$.

We then show in Fig. 3(a) and Fig. 3(b) the variations of P_{cov} and P_{con} with the interferer density λ under Rayleigh fading channels. Again, a good match between the simulation and theoretical results is observed in both Fig. 3(a) and Fig. 3(b). It is worth noting that although only the approximate theoretical models are obtained under Rayleigh fading channels, these models are still effective in modeling the network performance under such fading channels.

We further show in Fig. 4(a) and Fig. 4(b) the variation of connection outage probability P_{con} with $d_{A,B}$ under AWGN and Rayleigh fading channels, respectively. It can be observed from Fig. 4 even when the distance $d_{A,B}$ varies in a large range, the simulation results always match closely with the theoretical results for both AWGN and Rayleigh fading channels. Thus, our theoretical models can provide a robust performance modeling for the concerned network under both AWGN and Rayleigh fading channels as well as a wide range of settings for parameters like the distance between users and wardens, the number of wardens, etc.

B. Comparison of EGC and MRC

Note that we assume each warden has only the statistical CSI for the channel from Alice to itself, so we employ the EGC technique in the super warden W_Z for colluding detection. From Remark 1 we can see that when each warden knows the instantaneous CSI for the channel from Alice to itself, the MRC technique can be adopted at W_Z to achieve an enhanced detection performance. We show in Fig. 5 the covert performance comparison between the EGC and MRC techniques under the variation of the interferers' power P_I and the settings of $m = 2$, $\lambda = 0.2$, $\alpha = 4$, $P_A = 1$ W, and $N_A = 2$. It is observed from Fig. 5 that as P_I increases, the covert outage probability of the MRC and EGC techniques first increases and then decreases for both types of channel models. The results in Fig. 5 indicate clearly that with the help the instantaneous CSI for Alice-warden channels, using the MRC technique can lead to a significant improvement in detection performance than that using the EGC technique.

C. Outage Performance Under AWGN and Rayleigh Channels

We plot Fig. 6 to demonstrate the impact of the transmit power P_A on the covert outage probability P_{cov} for different values of m, with $\alpha = 4$, $\lambda = 0.09$ and $P_I = 1$ W. As depicted in Fig. 6, the covert outage probability increases monotonically with the increment of P_A under both the AWGN and Rayleigh channels. This observation is consistent with the findings presented in Proposition 2. We also observe that under the same conditions, the covert outage probability in the Rayleigh fading channel is higher compared to that in the AWGN channel, and the disparity between the two channels becomes more pronounced at higher values of P_A. This indicates that an increase in transmit power has a more substantial impact on covert performance under Rayleigh fading conditions. Additionally, it is worth noting that as the collusion intensity increases, the covert outage probability in both channels rises, suggesting that an increase in the number of colluding wardens negatively affects the performance of covert communications.

We plot Fig. 7 to show the impact of the collusion intensity m on the covert outage probability P_{cov} for different values of M, with $\alpha = 2.5$, $\lambda = 0.09$, $P_A = 0.1$ W and $P_I = 0.1$ W. We can see from Fig. 7 that the covert outage probability of under two channel models increases with the growth of the collusion intensity. The impact of the total number of wardens on covert outage probability is more significant under the Rayleigh channel compared to the AWGN channel.

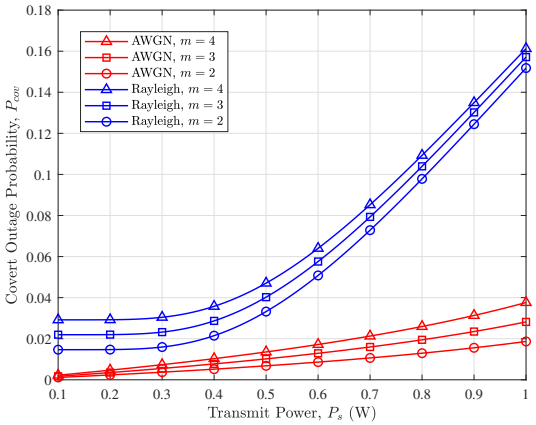

Fig. 6. Covert outage probability P_{cov} versus transmit power P_A for different values of m. $\alpha = 4$, $\lambda = 0.09$ and $P_I = 1$ W.

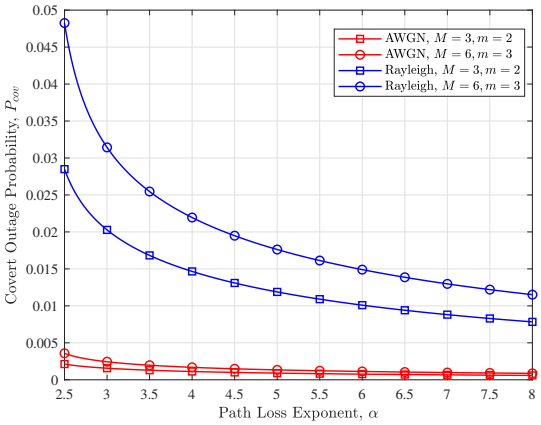

Fig. 8. Covert outage probability P_{cov} versus path loss exponent α for different values of M and m. $\lambda = 0.09$, $P_A = 0.1$ W and $P_I = 0.1$ W.

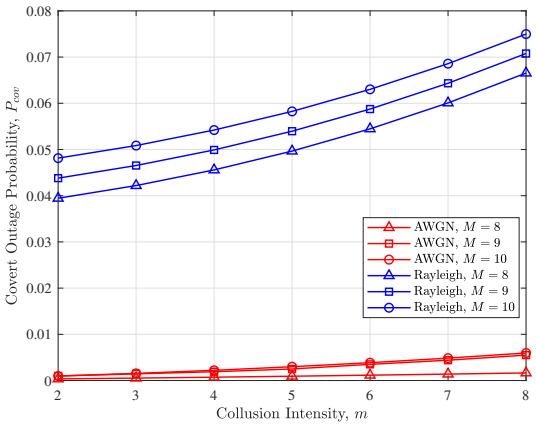

Fig. 7. Covert outage probability P_{cov} versus collusion intensity m for different values of M. $\alpha = 2.5$, $\lambda = 0.09$, $P_A = 0.1$ W and $P_I = 0.1$ W.

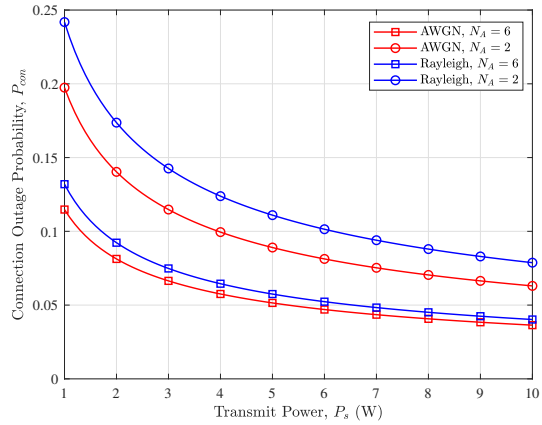

Fig. 9. Connection outage probability P_{con} versus transmit power P_A for different values of N_A. $\alpha = 4$, $\lambda = 0.09$ and $P_I = 1$ W.

Another careful observation is that the increase of the total number of wardens has a negative effect on the covert outage performance. The reason is that as the total number of wardens increases, the wardens will be more powerful to detect the covert communication.

We plot Fig. 8 to show the impact of the path loss exponent α on the covert outage probability P_{cov} for different values of M and m, with $\lambda = 0.09$, $P_A = 0.1$ W and $P_I = 0.1$ W. Fig. 8 indicates that the covert outage probability decreases as the path loss exponent increases for both channels. Additionally, under consistent channel conditions, larger values of M and m result in a more gradual decrease of this trend. It is also observed that the covert outage probability of Rayleigh channels is generally higher than that of AWGN channels for a given setting of α. This can be attributed to Rayleigh channels typically representing more adverse transmission conditions.

In Fig. 9, we illustrate the impact of the transmit power P_A on the connection outage probability P_{con} for different values of N_A, with $\alpha = 4$, $\lambda = 0.09$ and $P_I = 1$ W. It can be observed from Fig. 9 that as P_A increases, P_{con} decreases under both the two channels. We also note that a relatively higher number of antennas leads to a lower connection outage probability, which indicates that antenna diversity has a positive effect on connection reliability. A more careful observation from Fig. 9 is that when the transmit power is at a high level, the impact of the number of antennas on connection outage is weakened.

D. Covert Throughput Under AWGN and Rayleigh Channels

We now plot Fig. 10 to explore the impact of the transmit rate R on the covert throughput η for different values of ϵ under the two channel models, where we set $\alpha = 4$, $\lambda = 0.09$, $N_A = 6$, $P_I = 0.1$ W, $M = 4$ and $m = 2$. We can see from Fig. 10 that as the transmit rate increases, the covert throughput under both two channels first increases to their maximum and then decreases. The reasons behind the phenomenon can be explained as follows. When the transmission rate is low, the connection outage probability is relatively small, and thus the covert throughput increases as the transmission rate increases. However, when the transmission rate is excessively high, the connection outage probability approaches 1, rendering covert transmission impossible at that moment. This observation is

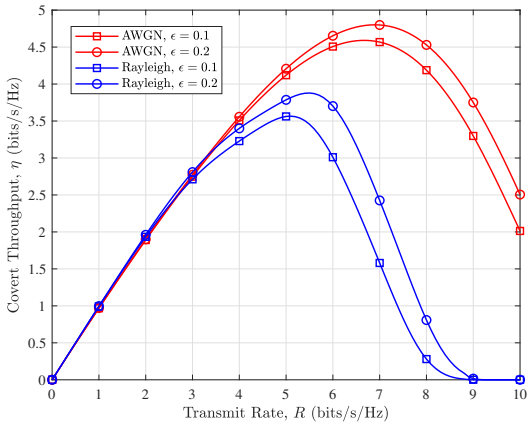

Fig. 10. Covert throughput η versus transmit rate R for different values of ϵ. $\alpha = 4$, $\lambda = 0.09$, $N_A = 6$, $P_I = 0.1$ W, $M = 4$ and $m = 2$.

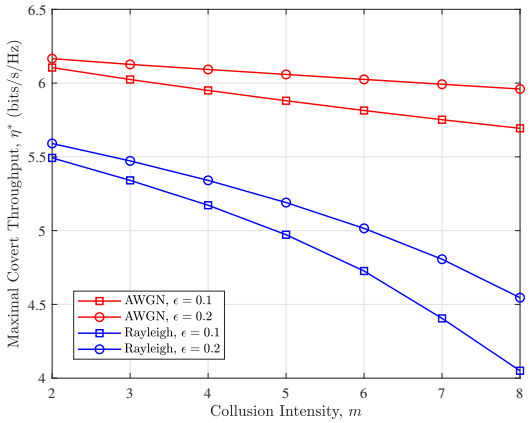

Fig. 11. Maximal covert throughput η^* versus collusion intensity m for different values of R. $\alpha = 4$, $\lambda = 0.09$, $N_A = 2$ and $P_I = 0.1$ W.

consistent with the findings presented in Proposition 3 and Theorem 3. We further observe from Fig. 10 that a relatively high covertness requirement threshold ϵ could lead to a big covert throughput under the both the two channels. This is because the increase of threshold leads to the increase of the optimal transmit power P_A^*, and thus the covert throughput η increases with ϵ.

Finally, we examine how the collusion intensity m affects the maximal covert throughput η^* under the two channel models, where we set $\alpha = 4$, $\lambda = 0.09$, $N_A = 2$ and $P_I = 0.1$ W. It can be observed from Fig. 11 that for both AWGN and Rayleigh channels, as the collusion intensity increases, the maximal covert throughput monotonically decreases. This indicates that higher collusion intensities have a negative impact on the maximal covert throughput. In addition, the maximal covert throughput in the AWGN channel is consistently higher than that in the Rayleigh channel for corresponding values of m and ϵ. This suggests that the AWGN channel is more robust against collusion impacts compared to the Rayleigh channel.

VI. Conclusion

This paper investigated the impact of warden collusion on covert communication in a multi-antenna wireless network with multiple wardens and interferers. Under typical AWGN and Rayleigh fading channels, we first presented the PDF and CDF of aggregate interference for non-colluding and colluding wardens using the Laplace transform and Cauchy Integral Theorem techniques. We then derived the expressions for the covert outage probability, connection outage probability, and covert throughput to reveal the intricate relationship between the collusion intensity m and these fundamental metrics of covert communication. To further reveal impact of warden collusion on the maximal covert throughput, we explored the joint optimization of transmit power and transmission rate to maximize covert throughput under specified covert outage requirements. Extensive numerical results were presented to demonstrate our theoretical models and indicate that warden collusion can significantly increase the covert outage possibility, thus deteriorate the covert communication performance. Another important finding of this paper is that under the same conditions with colluding wardens, the covert communication in AWGN channels is more stable and efficient than that in Rayleigh channels.

Appendix A
Proof of Lemma 2

Here, we apply mathematical induction to prove Lemma 2. When $m = 2$, expression (52) is reformulated as

$$(-1)^{m-2}\frac{1}{\prod_{\tau=1}^{m-1}(\mu_m - \mu_\tau)} = \frac{1}{\mu_2 - \mu_1}, \tag{66}$$

which means it always holds. We assume that expression (52) holds for $m = k$. In the following, we prove that when $m = k + 1$, expression (52) still holds.

$$\begin{aligned}
&(-1)^{k-1}\frac{1}{\prod_{\tau=1}^{k}(\mu_{k+1} - \mu_\tau)} \\
=&(-1)^{k-2}\frac{1}{\prod_{\tau=3}^{k}(\mu_{k+1} - \mu_\tau)}\left(\frac{1}{(\mu_{k+1} - \mu_1)(\mu_2 - \mu_1)}\right. \\
&\left. - \frac{1}{(\mu_{k+1} - \mu_2)(\mu_2 - \mu_1)}\right) \\
=&\frac{1}{(\mu_{k+1} - \mu_k)(\mu_{k+1} - \mu_{k-1})} \\
&\left(\frac{1}{(\mu_{k+1} - \mu_1)\prod_{v=2}^{k-2}(\mu_v - \mu_1)} - \frac{1}{(\mu_{k+1} - \mu_2)}\right. \\
&\frac{1}{\prod_{v=3}^{k-2}(\mu_v - \mu_2)(\mu_2 - \mu_1)} \\
&\left. + \ldots + (-1)^{k-3}\frac{1}{(\mu_{k+1} - \mu_{k-2})\prod_{\tau=1}^{k-3}(\mu_{k-2} - \mu_\tau)}\right)
\end{aligned}$$

$$
\begin{aligned}
=&\frac{1}{\mu_{k+1}-\mu_k}\left(\frac{(\mu_{k+1}-\mu_1)-(\mu_k-\mu_1)}{\prod_{v=2}^{k+1}(\mu_v-\mu_1)}\right.\\
&-\frac{(\mu_{k+1}-\mu_2)-(\mu_k-\mu_2)}{\prod_{v=3}^{k+1}(\mu_v-\mu_2)(\mu_2-\mu_1)}\\
&\left.+...+(-1)^{k-1}\frac{1}{(\mu_{k+1}-\mu_k)\prod_{\tau=1}^{k-1}(\mu_k-\mu_i)}\right)\\
=&\frac{1}{\prod_{v=2}^{k+1}(\mu_v-\mu_1)}\\
&-\frac{1}{\prod_{v=3}^{k+1}(\mu_v-\mu_2)(\mu_2-\mu_1)}+...\\
&+(-1)^{k-1}\frac{1}{\prod_{v=k+1}^{k+1}(\mu_v-\mu_k)\prod_{\tau=1}^{k-1}(\mu_k-\mu_\tau)}. \qquad (67)
\end{aligned}
$$

This completes the proof.

Appendix B
Proof of Theorem 1

We use mathematical induction to prove Theorem 1. First, we show that Theorem 1 is true for $m=2$. We have

$$
\begin{aligned}
f_{U_Z}(x)&=\int_{-\infty}^{+\infty}f_{U_{W_1}}(a)f_{U_{W_2}}(x-a)\,da\\
&=\int_0^x\mu_1e^{-\mu_1a}\mu_2e^{-\mu_2(x-a)}\,da\\
&=\mu_1\mu_2(\frac{e^{-\mu_1x}}{\mu_2-\mu_1}-\frac{e^{-\mu_2x}}{\mu_2-\mu_1}). \qquad (68)
\end{aligned}
$$

Assuming that Theorem 1 holds when $m=k$, then we only need verify that Theorem 1 holds when $m=k+1$. By using the properties of exponential distribution [45], we have

$$
\begin{aligned}
&f_{U_Z}(x)=\int_{-\infty}^{+\infty}f_{U_{W_{k+1}}}(a)f_{U_{W_1+...+W_k}}(x-a)\,da\\
&=\int_0^x\mu_{k+1}e^{-\mu_{k+1}x}\prod_{v=1}^{k}\mu_v\left(\frac{e^{-\mu_1(x-a)}}{\prod_{v=2}^{k}(\mu_v-\mu_1)}-\right.\\
&\left.\frac{e^{-\mu_2(x-a)}}{\prod_{v=3}^{k}(\mu_v-\mu_2)(\mu_2-\mu_1)}+...+\frac{(-1)^{k-1}e^{-\mu_k(x-a)}}{\prod_{\tau=1}^{k-1}(\mu_k-\mu_\tau)}\right)da\\
&=\prod_{v=1}^{k+1}\mu_v\left(\frac{e^{-\mu_1x}}{\prod_{v=2}^{k}(\mu_v-\mu_1)}\int_0^x e^{-(\mu_{k+1}-\mu_1)a}\,da+...+\right.\\
&\left.(-1)^{k-1}\frac{e^{-\mu_kx}}{\prod_{\tau=1}^{k-1}(\mu_k-\mu_\tau)}\int_0^x e^{-(\mu_{k+1}-\mu_k)a}\,da\right)\\
&=\prod_{v=1}^{k+1}\mu_v\left(\frac{e^{-\mu_1x}}{\prod_{v=2}^{k+1}(\mu_v-\mu_1)}-\frac{e^{-\mu_2x}}{\prod_{v=3}^{k+1}(\mu_v-\mu_2)(\mu_2-\mu_1)}\right.\\
&+...+\frac{e^{-\mu_{k+1}x}}{\prod_{v=2}^{k+2}(\mu_v-\mu_1)}-\frac{e^{-\mu_{k+1}x}}{\prod_{v=3}^{k+2}(\mu_v-\mu_2)(\mu_2-\mu_1)}\\
&\left.+...+(-1)^k\frac{e^{-\mu_{k+1}x}}{\prod_{v=k+2}^{k+2}(\mu_v-\mu_{k+1})\prod_{\tau=1}^{k}(\mu_{k+1}-\mu_\tau)}\right)\\
&\overset{(d)}{=}\prod_{v=1}^{k+1}\mu_v\left(\frac{e^{-\mu_1x}}{\prod_{v=2}^{k+1}(\mu_v-\mu_1)}-\frac{e^{-\mu_2x}}{\prod_{v=3}^{k+1}(\mu_v-\mu_2)(\mu_2-\mu_1)}\right.\\
&\left.+...+(-1)^k\frac{e^{-\mu_{k+1}x}}{\prod_{\tau=1}^{k}(\mu_{k+1}-\mu_\tau)}\right). \qquad (69)
\end{aligned}
$$

where (d) is due to Lemma 2. Thus, the proof is completed.

References

[1] A. J. Menezes, P. C. Van Oorschot, and S. A. Vanstone, *Handbook of applied cryptography*. CRC press, 2018.

[2] N. Yang, L. Wang, G. Geraci, M. Elkashlan, J. Yuan, and M. Di Renzo, "Safeguarding 5G wireless communication networks using physical layer security," *IEEE Commun. Mag.*, vol. 53, no. 4, pp. 20–27, Apr. 2015.

[3] S. Yan, X. Zhou, J. Hu, and S. V. Hanly, "Low probability of detection communication: Opportunities and challenges," *IEEE Wireless Commun.*, vol. 26, no. 5, pp. 19–25, Oct. 2019.

[4] N. F. Johnson and S. Katzenbeisser, "A survey of steganographic techniques," in *Proc. Information hiding*, 2000, pp. 43–78.

[5] P. H. Che, M. Bakshi, and S. Jaggi, "Reliable deniable communication: Hiding messages in noise," in *Proc. IEEE Int. Symp. Information Theory (ISIT)*, 2013, pp. 2945–2949.

[6] B. A. Bash, D. Goeckel, and D. Towsley, "Limits of reliable communication with low probability of detection on AWGN channels," *IEEE J. Sel. Areas Commun.*, vol. 31, no. 9, pp. 1921–1930, Sep. 2013.

[7] Y. Wang, S. Yan, W. Yang, Y. Huang, and C. Liu, "Energy-efficient covert communications for bistatic backscatter systems," *IEEE Trans. Veh. Technol.*, vol. 70, no. 3, pp. 2906–2911, Mar. 2021.

[8] S. Yan, S. V. Hanly, and I. B. Collings, "Optimal transmit power and flying location for UAV covert wireless communications," *IEEE J. Sel. Areas Commun.*, vol. 39, no. 11, pp. 3321–3333, Nov. 2021.

[9] C. Wang, X. Chen, J. An, Z. Xiong, C. Xing, N. Zhao, and D. Niyato, "Covert communication assisted by UAV-IRS," *IEEE Trans. Commun.*, vol. 71, no. 1, pp. 357–369, Jan. 2022.

[10] S. Qiao, D. Cao, Q. Zhang, Y. Xu, and G. Liu, "Covert communication gains from adversary's uncertainty of phase angles," *IEEE Trans. Inf. Forensics Security*, vol. 18, pp. 2899–2912, May 2023.

[11] L. Yang, W. Zhang, P. S. Bithas, H. Liu, M. O. Hasna, T. A. Tsiftsis, and D. W. K. Ng, "Covert transmission and secrecy analysis of RS-RIS-NOMA-aided 6G wireless communication systems," *IEEE Trans. Veh. Technol.*, vol. 72, no. 8, pp. 10 659–10 670, Aug. 2023.

[12] K. Shahzad, X. Zhou, S. Yan, J. Hu, F. Shu, and J. Li, "Achieving covert wireless communications using a full-duplex receiver," *IEEE Trans. Wireless Commun.*, vol. 17, no. 12, pp. 8517–8530, Dec. 2018.

[13] M. T. Mamaghani and Y. Hong, "Aerial intelligent reflecting surface-enabled terahertz covert communications in beyond-5G Internet of Things," *IEEE Internet Things J.*, vol. 9, no. 19, pp. 19 012–19 033, Oct. 2022.

[14] Y. Zhang, L. Yang, X. Li, K. Guo, and H. Liu, "Covert communications for STAR-RIS-assisted industrial networks with a full duplex receiver and RSMA," *IEEE Internet Things J.*, vol. 11, no. 12, pp. 22 483–22 493, Jun. 2024.

[15] H. Mao, Y. Liu, Z. Xiao, Z. Han, and X.-G. Xia, "Joint resource allocation and 3-D deployment for multi-UAV covert communications," *IEEE Internet Things J.*, vol. 11, no. 1, pp. 559–572, Jan. 2024.

[16] M. Forouzesh, P. Azmi, N. Mokari, and D. Goeckel, "Covert communication using null space and 3D beamforming: Uncertainty of willie's location information," *IEEE Trans. Veh. Technol.*, vol. 69, no. 8, pp. 8568–8576, Aug. 2020.

[17] S. Ma, H. Sheng, R. Yang, H. Li, Y. Wu, C. Shen, N. Al-Dhahir, and S. Li, "Covert beamforming design for integrated radar sensing and communication systems," *IEEE Trans. Wireless Commun.*, vol. 22, no. 1, pp. 718–731, Jan. 2022.

[18] Y. Zhang, Y. Zhang, J. Wang, S. Xiao, and W. Tang, "Distance-angle beamforming for covert communications via frequency diverse array: Toward two-dimensional covertness," *IEEE Trans. Wireless Commun.*, vol. 22, no. 12, pp. 8559–8574, Dec. 2023.

[19] J. Xing, T. Lv, W. Li, W. Ni, and A. Jamalipour, "Joint optimization of beamforming and noise injection for covert downlink transmissions in cell-free internet of things networks," *IEEE Internet Things J.*, vol. 11, no. 6, pp. 10 525–10 536, Mar. 2024.

[20] L. Lv, Z. Li, H. Ding, N. Al-Dhahir, and J. Chen, "Achieving covert wireless communication with a multi-antenna relay," *IEEE Trans. Inf. Forensics Security*, vol. 17, pp. 760–773, Feb. 2022.

[21] M. Wang, Z. Xu, B. Xia, Y. Guo, and Z. Chen, "DF relay assisted covert communications: Analysis and optimization," *IEEE Trans. Veh. Technol.*, vol. 72, no. 3, pp. 4073–4078, Mar. 2023.

[22] D. Deng, X. Li, S. Dang, M. C. Gursoy, and A. Nallanathan, "Covert communications in intelligent reflecting surface-assisted two-way relaying networks," *IEEE Trans. Veh. Technol.*, vol. 71, no. 11, pp. 12 380–12 385, Nov. 2022.

[23] C. Gao, B. Yang, D. Zheng, X. Jiang, and T. Taleb, "Cooperative jamming and relay selection for covert communications in wireless relay systems," *IEEE Trans. Commun.*, vol. 72, no. 2, pp. 1020–1032, Feb. 2024.

[24] M. Lin, C. Liu, and W. Wang, "Relay-assisted uplink covert communication in the presence of multi-antenna warden and uninformed jamming," *IEEE Trans. Commun.*, vol. 72, no. 4, pp. 2124–2137, Apr. 2024.

[25] B. Wang, Y. Zhang, R. Xu, S. Jiang, A. Liu, G. Ding, and X. Liang, "Relay-assisted finite blocklength covert communications for internet of things," *IEEE Internet Things J.*, 2024.

[26] R. Ma, W. Yang, X. Guan, X. Lu, Y. Song, and D. Chen, "Covert mmwave communications with finite blocklength against spatially random wardens," *IEEE Internet Things J.*, vol. 11, no. 2, pp. 3402–3416, Jan. 2024.

[27] Y. Jiang, L. Wang, and H.-H. Chen, "Covert communications with randomly distributed adversaries in wireless energy harvesting enabled D2D underlaying cellular networks," *IEEE Trans. Inf. Forensics Security*, vol. 18, pp. 5401–5415, Aug. 2023.

[28] S. Feng, X. Lu, S. Sun, D. Niyato, and E. Hossain, "Securing large-scale D2D networks using covert communication and friendly jamming," *IEEE Trans. Wireless Commun.*, vol. 23, no. 1, pp. 592–606, Jan. 2024.

[29] S. Zhao, J. Liu, Y. Shen, and X. Jiang, "Covert outage analysis for random wireless networks under warden collusion," in *Proc. IEEE International Conference on Networking and Network Applications (NaNA)*, 2020, pp. 193–197.

[30] R. Ma, W. Yang, L. Tao, X. Lu, Z. Xiang, and J. Liu, "Covert communications with randomly distributed wardens in the finite blocklength regime," *IEEE Trans. Veh. Technol.*, vol. 71, no. 1, pp. 533–544, Jan. 2021.

[31] A. Arghavani, S. Dey, and A. Ahlén, "Covert outage minimization in the presence of multiple wardens," *IEEE Trans. Signal Process.*, vol. 71, pp. 686–700, Feb. 2023.

[32] H. Jia, L. Ma, and D. Qin, "Robust beamforming design for covert integrated sensing and communication in the presence of multiple wardens," *IEEE Trans. Veh. Technol.*, vol. 73, no. 11, pp. 17 135–17 150, Nov. 2024.

[33] M. Forouzesh, P. Azmi, A. Kuhestani, and P. L. Yeoh, "Covert communication and secure transmission over untrusted relaying networks in the presence of multiple wardens," *IEEE Trans. Commun.*, vol. 68, no. 6, pp. 3737–3749, Jun. 2020.

[34] D. Hamza, S. Aïssa, and G. Aniba, "Equal gain combining for cooperative spectrum sensing in cognitive radio networks," *IEEE Trans. Wireless Commun.*, vol. 13, no. 8, pp. 4334–4345, Aug. 2014.

[35] H. Kong, M. Lin, J. Zhang, J. Ouyang, W.-P. Zhu, and M.-S. Alouini, "Beamforming design and performance analysis for satellite and UAV integrated networks in IoRT applications," *IEEE Internet Things J.*, vol. 9, no. 16, pp. 14 965–14 977, Aug. 2022.

[36] Y. Xu, L. Xie, D. Xu, and S. Song, "Fundamental limits and base station selection for collaborative sensing in perceptive mobile networks," in *Proc. IEEE International Mediterranean Conference on Communications and Networking (MeditCom)*, 2023, pp. 97–102.

[37] I. Barhumi, G. Leus, and M. Moonen, "Optimal training design for MIMO OFDM systems in mobile wireless channels," *IEEE Trans. Signal Process.*, vol. 51, no. 6, pp. 1615–1624, Jun. 2003.

[38] Y. Liu, Z. Tan, H. Hu, L. J. Cimini, and G. Y. Li, "Channel estimation for OFDM," *IEEE Commun. Surv. Tutor.*, vol. 16, no. 4, pp. 1891–1908, 2014.

[39] B. He, S. Yan, X. Zhou, and H. Jafarkhani, "Covert wireless communication with a poisson field of interferers," *IEEE Trans. Wireless Commun.*, vol. 17, no. 9, pp. 6005–6017, Sep. 2018.

[40] Y. Zhang, Y. Shen, H. Wang, J. Yong, and X. Jiang, "On secure wireless communications for IoT under eavesdropper collusion," *IEEE Trans. Autom. Sci. Eng.*, vol. 13, no. 3, pp. 1281–1293, Jul. 2016.

[41] T. Zheng, H. Wang, D. W. K. Ng, and J. Yuan, "Multi-antenna covert communications in random wireless networks," *IEEE Trans. Wireless Commun.*, vol. 18, no. 3, pp. 1974–1987, Mar. 2019.

[42] S. Yan, B. He, X. Zhou, Y. Cong, and A. L. Swindlehurst, "Delay-intolerant covert communications with either fixed or random transmit power," *IEEE Trans. Inf. Forensics Security*, vol. 14, no. 1, pp. 129–140, Jan. 2019.

[43] T.-X. Zheng, Z. Yang, C. Wang, Z. Li, J. Yuan, and X. Guan, "Wireless covert communications aided by distributed cooperative jamming over slow fading channels," *IEEE Trans. Wireless Commun.*, vol. 20, no. 11, pp. 7026–7039, Nov. 2021.

[44] M. Haenggi, J. G. Andrews, F. Baccelli, O. Dousse, and M. Franceschetti, "Stochastic geometry and random graphs for the analysis and design of wireless networks," *IEEE J. Sel. Areas Commun.*, vol. 27, no. 7, pp. 1029–1046, Sep. 2009.

[45] E. T. Jaynes, *Probability theory: The logic of science*. Cambridge university press, 2003.

Shuangrui Zhao (Member, IEEE) received the B.S. degree and Ph.D. degree from Xidian University in 2015 and 2021, respectively. He is currently an Associate Professor with the School of Computer Science and Technology, Xidian University. His research interests include physical layer security of wireless communications and optimal control.

Jia Liu (Senior Member, IEEE) received the B.E. degree from the School of Telecommunications Engineering, Xidian University, Xi'an, China, in 2010, and received the Ph.D. degree from the School of Systems Information Science, Future University Hakodate, Japan, in 2016. His research interests include wireless systems security, space-air-ground integrated networks, Internet of Things, 6G, etc.

Yulong Shen (Member, IEEE) received the B.S. and M.S. degrees in computer science and Ph.D. degree in cryptography from Xidian University, Xi'an, China, in 2002, 2005, and 2008, respectively. He is currently a Professor with the School of Computer Science and Technology, Xidian University, where he is also an Associate Director of the Shaanxi Key Laboratory of Network and System Security and a member of the State Key Laboratory of Integrated Services Networks. His research interests include wireless network security and cloud computing security. He has also served on the technical program committees of several international conferences, including ICEBE, INCoS, CIS, and SOWN.

Xiaohong Jiang (Senior Member, IEEE) received his B.S., M.S. and Ph.D degrees in 1989, 1992, and 1999 respectively, all from Xidian University, China. He is currently a full professor of Future University Hakodate, Japan. Before joining Future University, Dr. Jiang was an Associate professor, Tohoku University, from Feb. 2005 to Mar. 2010. Dr. Jiang's research interests mainly include wireless networks, network security, optical networks, router/switch design, etc. He has published over 300 technical papers at premium international journals and conferences, which include over 80 papers published in top IEEE journals and top IEEE conferences, like the IEEE/ACM Transactions on Networking (TON), the IEEE Journal of Selected Areas on Communications (JSAC), the IEEE INFOCOM.

Tarik Taleb (Senior Member, IEEE) received the B.E. degree (with distinction) in information engineering and the M.Sc. and Ph.D. degrees in information sciences from Tohoku University, Sendai, Japan, in 2001, 2003, and 2005, respectively. He is currently a Full Professor at Ruhr University Bochum, Germany. He was a Professor with the Center of Wireless Communications, University of Oulu, Oulu, Finland. He is the founder of ICTFICIAL Oy, and the founder and the Director of the MOSA!C Lab, Espoo, Finland. From October 2014 to December 2021, he was an Associate Professor with the School of Electrical Engineering, Aalto University, Espoo, Finland. Prior to that, he was working as a Senior Researcher and a 3GPP Standards Expert with NEC Europe Ltd., Heidelberg, Germany. Before joining NEC and till March 2009, he worked as Assistant Professor with the Graduate School of Information Sciences, Tohoku University, in a lab fully funded by KDDI. From 2005 to 2006, he was a Research Fellow with the Intelligent Cosmos Research Institute, Sendai. Taleb has been directly engaged in the development and standardization of the Evolved Packet System as a member of the 3GPP System Architecture Working Group. His current research interests include AI-based network management, architectural enhancements to mobile core networks, network softwarization and slicing, mobile cloud networking, network function virtualization, software-defined networking, software-defined security, and mobile multimedia streaming.

Norio Shiratori (Life Fellow, IEEE) received his Ph.D. degree from Tohoku University in 1977. He became an Assistant Professor and Associate Professor at the Research Institute of Electrical Communication, Tohoku University, in 1977 and 1984, respectively. In 1990, he was promoted to Full Professor at the School of Engineering, Tohoku University. In 1993, he commenced his role as Full Professor at the Research Institute of Electrical Communication, Tohoku University. In 1997, Prof. Shiratori became a Visiting Professor at UCLA (University of California, Los Angeles). In 1998, he was elevated to the status of IEEE Fellow. In 2004, Prof. Shiratori assumed the role of Japan representative for the International Federation for Information Processing (IFIP). In 2009, he served as the President of the Information Processing Society of Japan. In 2010, following his retirement from Tohoku University, Prof. Shiratori took on the positions of Professor Emeritus at Tohoku University and Board Member at Future University Hakodate. In the same year, he became the Chair of the IEEE Sendai Section. In 2012, he was appointed as a Professor at the Global Information and Telecommunication Institute, Waseda University. In 2013, Prof. Shiratori assumed the role of Vice Chair of the IEEE Japan Council. Recognizing his significant contributions, he was honored with the title of IEEE Life Fellow in 2017. Since 2017, he has been serving as a Professor at Research and Development Initiative, Chuo University. Prof. Shiratori has published over 15 books and over 600 refereed papers in computer science and related fields. He is a fellow of the Japan Foundation of Engineering Societies (JFES), the Information Processing Society of Japan (IPSJ), and the Institute of Electronics, Information and Communication Engineers (IEICE). He was a recipient of the Minister of MEXT Award from the Japanese Government in 2016, the Science and Technology Award from the Ministry of Education, Culture, Sports, Science, and Technology (MEXT) in 2009.